NIST
National Institute of Standards and Technology
Technology Administration, U.S. Department of Commerce

NIST Technical Note 1538

Optimized Arbitrary Wireless Device Arrays for Emergency Response Communications

William F. Young
Edward F. Kuester
Christopher L. Holloway

NIST Technical Note 1538

Optimized Arbitrary Wireless Device Arrays for Emergency Response Communications

William F. Young
Sandia National Laboratory
Networked Systems Survivability and Assurance Department
Albuquerque, NM 87185

Edward F. Kuester
Department of Electrical and Computing Engineering
University of Colorado
Boulder, CO 80309

Christopher L. Holloway
Electromagnetics Division
National Institute of Standards and Technology
Boulder, CO 80305

March 2005

U.S. Department of Commerce
Carlos M. Gutierrez, Secretary

Technology Administration
Phillip J. Bond, Under Secretary for Technology

National Institute of Standards and Technology
Hratch G. Semerjian, Acting Director

Certain commercial entities, equipment, or materials may be identified in this document in order to describe an experimental procedure or concept adequately. Such identification is not intended to imply recommendation or endorsement by the National Institute of Standards and Technology, nor is it intended to imply that the entities, materials, or equipment are necessarily the best available for the purpose.

National Institute of Standards and Technology Technical Note 1538
Natl. Inst. Stand. Technol. Tech. Note 1538, 49 pages (March 2005)
CODEN: NTNOEF

U.S. Government Printing Office
Washington: 2005

For sale by the Superintendent of Documents, U.S. Government Printing Office
Internet bookstore: gpo.gov Phone: 202-512-1800 Fax: 202-512-2250
Mail: Stop SSOP, Washington, DC 20402-0001

Contents

Executive Summary iv

1 Introduction 2

2 Basic Theory 3

3 Simulation Setup 9

4 Simulation Results 14

4.1 Average Gain with Elements in a Plane and Interior Observation Points 14

4.2 Effect of Current Magnitude on Optimized Gain 18

4.3 Effect of Current Phase on Optimized Gain 21

4.4 Average Gain with Elements in a Plane and Exterior Observation Points 23

4.5 Effect of Elements Located in a Volume versus a Plane 26

5 Conclusions and Future Work 37

6 References 38

Appendix A: Examination of Statistics Gathering Method 40

Executive Summary

Wireless communications are essential to emergency responders. Unfortunately, a typical emergency response scenario involves communication into and within building structures, which can severely interfere with or completely block the radio-frequency channel. Several methods offer some potential relief to these problems, including the use of multi-hop ad hoc networks for communication within the building, and the use of smart antenna arrays at exterior locations to improve the communication between the interior and exterior locations of the building. However, due to the enclosed nature of buildings, and the loss in radio-frequency energy as a signal propagates through floors and walls, no single solution completely solves the communication problem.

In this report, we consider another approach to improving the communication capabilities of emergency responders. We investigate the possibility of creating antenna arrays from wireless devices such as the emergency responders' radios, wireless sensor networks, or arbitrarily placed wireless relay nodes. An antenna array allows the focusing or directing of radiated electromagnetic energy in a desired direction. By intelligently controlling the direction and energy level of the electromagnetic radiation, we can increase the probability of establishing a communication link and improve the quality of that link. The result improves the emergency responder's communication capabilities.

Our approach is based on antenna array theory. However, unlike the typical assumption that the observation point or responder is located in the far field of the array, we assume the responder is located within or near the array volume. The array volume is essentially the building. We also assume arbitrarily located wireless devices, which are in effect the antenna array elements. This initial investigation shows gain is possible from arbitrarily located wireless nodes, at frequencies between 100 MHz to 5 GHz. The results also indicate gain is possible whether the emergency responder is moving through the interior of the building, or moving around the perimeter of the building. This means the array concept could provide benefit to emergency responders within the building, and to

emergency responders communicating with people on the exterior of the building. We also point out our approach is not based on ad hoc networking or protocols. Although an actual system will make use of such protocols, we are focusing on the electromagnetic behavior of the system in aggregate.

The preliminary results discussed here are encouraging. We also continue to improve our model of the real world environment by refining the approximation used for the building materials, such as the floor of the building. In addition, in an actual implementation, emergency responders would likely quickly place wireless devices as they enter the building, or perhaps even robots could place the devices in the near future. We are investigating possible benefits from any inherent structure or pattern that arises from the placement of the wireless devices, or from probable locations within the building.

Optimized Arbitrary Wireless Device Arrays for Emergency Response Communications

William F. Young[1] Edward F. Kuester[2] Christopher L. Holloway[3]

National Institute of Standards and Technology
325 Broadway, Boulder CO 80305

In typical emergency response situations wireless communications are essential to the emergency responders. However, a typical scenario requires communicating into and within building structures that may severely interfere with or completely block the radio-frequency channel. In this report, we are investigating the potential of utilizing arbitrarily located wireless devices to increase the probability of maintaining a communication link between two points and thus improve the emergency responder's communication capabilities. The proposed approach employs methods based in antenna array and general optimization theory. A combination of analytic and simulation results allows rapid and efficient analysis of a variety of array or system configurations. In order to investigate general trends, we approximate the floor of the building as a perfect electrical conductor and the wireless devices as Hertzian dipole elements. Observation points are located throughout the notional building volume, as well as on a perimeter zone. An important aspect of our analytic solution considers the observation points as being in the far field of the individual radiating elements, with the gain normalized by the system input power. The initial analytic and simulation results lead to the following general conclusions. First, an appropriately controlled system of wireless devices can increase the communication capability within a building by optimizing the directivity of electromagnetic radiation. Second, the emergency responder can move throughout the building and surrounding area, and receive similar benefit from the array of elements. Third, the optimized current phase information demonstrates a greater affect on the amount of achievable gain when compared to the optimized current magnitude information.

Keywords: Emergency responder; random antenna array; optimization; wireless devices

---

[1] Sandia National Laboratories, PO Box 5800, MS 0785, Albuquerque, NM, 87185, email: wfyoung@sandia.gov
[2] University of Colorado, Boulder, CO
[3] Electromagnetics Division, NIST, MC 818.02, email: holloway@boulder.nist.gov

1. Introduction

Wireless communication represents a key supporting technology to the success of an emergency responder. Unfortunately, a typical emergency response scenario involves communication into building structures, which can severely interfere with or completely block the radio-frequency channel. One potential method of improving the radio frequency channel within a building utilizes the intelligent control of the electromagnetic radiation from wireless devices quickly placed in the building during entry by the emergency responder. These devices would perform as antenna array elements to improve communication capability for emergency responders both within the structure and with external persons.

We here investigate the potential for creating directive arrays out of arbitrarily located radio transceivers. These transceivers may take a variety of forms such as handheld radios, wireless relay devices, or sensor nodes. The goal is to direct the electromagnetic energy for particular radio-frequency channels within a large volume area, (e.g., a large building), so as to improve both the coverage and/or data throughput of the wireless communication channel between two points. This research is intended to directly improve the design of wireless communication systems used in current and future emergency response scenarios.

Our approach applies optimization techniques and antenna array theory to arbitrarily located radiating elements. Optimization techniques for arrays of discrete radiators have a rich history, with References [1] through [3] detailing optimization techniques for scalar radiation from discrete radiators and chapter 10 in Reference [4] providing a discussion particularly relevant to this work. In addition, Reference [5] provides a highly mathematical approach to the problem of optimizing electromagnetic radiation in a particular direction. References [6] through [9] consider probabilistic approaches to antenna array design, while References [10] and [11] investigate the effects due to random variation from initial optimized parameters such as element location and current

excitation. However, to the best of our knowledge, the application of array theory concepts to arbitrarily located wireless transceivers represents a new area of investigation. In this preliminary report, we examine the feasibility of having the observation point at a variety of locations within or near the array. The observation point is analogous to an emergency responder trying to receive a transmission within a building that also contains numerous wireless devices, which constitute the array elements. Observation points on the perimeter of the facility also provide an important investigation emphasis since communication will occur not only between emergency responders within the building, but with persons outside of the building as well.

Our proposed topology of wireless devices resembles an ad hoc network, but our focus is not on ad hoc networks or protocols. We are studying the possibility of controlling the electromagnetic radiation of the wireless devices in aggregate so as to form an antenna array. This differs from the typical power control of a single device, which is used simply either to restrict or expand its radius of coverage, or to increase the battery life by limiting usage. A complete system using our approach will require various supporting protocols; however, our goal is to determine the necessary electromagnetic behavior of the system.

The remainder of the report proceeds as follows. In Section 2, we outline the basic underlying theory behind our approach; in Section 3, we describe the general simulation setup and scenarios; in Section 4, we expand on further specifics for particular simulations and draw important corresponding results; and finally, in Section 5, we present some overall conclusions and ideas for future work.

2. Basic Theory

Basic concepts from antenna array theory serve as the starting point for the analytical basis of optimizing the electromagnetic radiation from arbitrarily located transceivers or elements. Optimizing the ratio of two characteristics associated with the elements is a

common approach used to determine the appropriate excitation and/or physical orientation of the elements. This work seeks to maximize the electromagnetic energy at a given observation point by determining the required current (magnitude and phase), on each element. In this work, we assume the locations of the arbitrarily located elements are known. Figure 1 provides an example of the physical configuration considered in the optimization process.

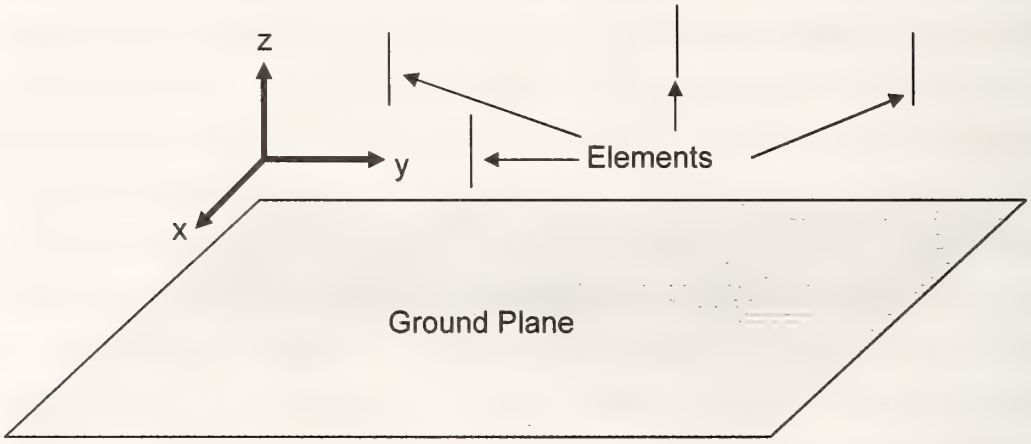

Figure 1. Example configuration with four z-directed dipoles over a ground plane.

The example configuration in figure 1 consists of four z-directed dipole elements over a perfect electric conductor (PEC) ground plane. In this analysis, the ground plane is assumed infinite in extent in both the x and y directions. The observation point lies in the vicinity of the elements ("vicinity" is defined as lying within the minimal volume containing the elements, or in the perimeter region surrounding the array). Two characteristics of the configuration are used in the optimization process: (1) the total power provided to the system, and (2) the z-directed radiation intensity at the observation point over the ground plane. The optimization involves setting up the ratio of these two

quantities, and then finding the complex current excitations that produce the greatest ratio.

Several typical measures of optimization apply to antenna arrays, (e.g., see Reference [12]). However, we want to optimize the electromagnetic radiation intensity for a particular direction, i.e., the z-direction, at a specific observation point within or near the boundaries of the array volume. The specific ratio necessary to optimize takes the form given below:

$$p = \frac{4\pi \cdot (\text{z}-\text{component of radiation intensity})}{\text{system input power}} = \frac{4\pi \dfrac{R_{ave}^2 \left| E_z(\bar{r}) \right|^2}{2\eta}}{-\dfrac{1}{2}\,\text{Re} \iiint \bar{E}(\bar{r}) \cdot \bar{J}^*(\bar{r})\, dv}, \quad (1)$$

where R_{ave} is the average distance between the elements and the observation point, E_z is the z-component of the electric field, η is the intrinsic impedance of free space, $\bar{E}$ is the electric field vector, $\bar{J}$ is the current vector, $\bar{r}$ is the distance vector from the origin, and dv is the volume differential. Distance R_{ave} is used because the observation point is either near or within the volume containing the array of elements, which suggests estimating the distance to the observation point by means other than the distance from the origin or center of the array to the observation point. Note that eq (1) is not exactly equivalent to the classical definition of antenna directivity, as given in eqs (2–16) of Reference [13], since that definition uses an R value corresponding to the far field of the array and assumes all the array elements are located at the origin. In our case, the distance between the observation points and the elements is not in the far field of the array, hence using R_{ave} provides a better mathematical representation of the overall behavior than simply using some nominal R value, such as the distance to the farthest observation point. Our goal is to maximize the value of p, which represents the gain in a specific direction.

The array of elements constitutes a discrete system, and both the numerator and denominator take the form of matrices. In addition, the numerator matrix is Hermitian,

and the denominator is Hermitian positive definite. This allows the application of classic optimization theory to determine the maximum value of p and the corresponding current excitations on the elements. Derivation of the Green's function, $\overline{\overline{G}}^z$, for a z-directed Hertzian dipole element over a PEC allows writing the volume integral in closed form. In particular, the electric field is written as

$$\bar{E}(\bar{r}) = \overline{\overline{G}}^z(\bar{r},\bar{r}_m) = G^z(\bar{r},\bar{r}_m)\hat{a}_z + \frac{1}{k^2}\nabla\nabla G^z(\bar{r},\bar{r}_m)\hat{a}_z, \tag{2}$$

where

$$G^z(\bar{r},\bar{r}_m) = \frac{e^{-jk|\bar{r}-\bar{r}_m|}}{4\pi|\bar{r}-\bar{r}_m|} + \frac{e^{-jk|\bar{r}-\bar{r}'_m|}}{4\pi|\bar{r}-\bar{r}'_m|}, \tag{3}$$

$$\bar{r}_m = \sqrt{(x-x_m)^2+(y-y_m)^2+(z-z_m)^2}, \quad (\text{m}^{\text{th}} \text{ dipole source location}) \tag{4}$$

$$\bar{r}'_m = \sqrt{(x-x_m)^2+(y-y_m)^2+(z+z_m)^2}, \quad (\text{image of the m}^{\text{th}} \text{ dipole source}) \tag{5}$$

and

$$\bar{r} = \sqrt{x^2+y^2+z^2}, \tag{6}$$

where $\bar{r}$ is the distance from the origin to the observation point. Other variables in eq (2) are k, which is the wavenumber, $j = \sqrt{-1}$, and $\hat{a}_z$, which is the unit vector in the z-direction. The m$^{\text{th}}$ Hertzian dipole current source, $\bar{J}_m$, generating this electric field is given as

$$\bar{J}_m = -\hat{a}_z \frac{\delta(\bar{r}-\bar{r}_m)}{j\omega\mu_0}, \tag{7}$$

where ω is the radian frequency, μ_0 it the permeability of free space, and $\delta(\cdot)$ is the impulse or delta function. By the sifting property of the delta function in the current source, and the dot product from the vector multiplication, the volume integral in eq (1) takes the form

$$-\frac{1}{2}\mathrm{Re}\iiint \bar{E}\cdot\bar{J}^{*}dv=\frac{1}{2}\mathrm{Re}\left\{\frac{j}{\omega\mu_0}\sum_{m=1}^{N}\sum_{n=1}^{N}G^{z}(\bar{r}_m,\bar{r}_n)+\frac{1}{k^2}\frac{\partial^2}{\partial z^2}G^{z}(\bar{r}_m,\bar{r}_n)\right\}. \tag{8}$$

Equation (8) is a square $N\times N$ matrix, where N is the number of source elements, i.e., four source elements means $N = 4$. Let B represent this denominator matrix. Now letting $R_a=|\bar{r}_m-\bar{r}_n|$ and $R_b=|\bar{r}_m'-\bar{r}_n|$, and taking the real part, the terms in matrix eq (8) may be written as

$$B_{m,n}=\frac{k}{8\pi\omega\mu_0}\left\{\frac{\sin(kR_a)}{kR_a}+\frac{\sin(kR_b)}{kR_b}+\frac{1}{k^2}\frac{\partial^2}{\partial z_n^{\,2}}\left[\frac{\sin(kR_a)}{kR_a}+\frac{\sin(kR_b)}{kR_b}\right]\right\}. \tag{9}$$

Almost all the terms in eq (9) can be written in closed form, (except for the self terms of R_a); hence, the closed form expression for the matrix terms in B is as follows:

$$B_{m,n}=\frac{k}{8\pi\omega\mu_0}\left\{\begin{aligned}&\frac{\sin(kR_a)}{kR_a}\left[1-\frac{(1+(z_n-z_m)^2k^2)}{k^2R_a^2}+\frac{3(z_n-z_m)^2}{k^2R_a^4}\right]\\&+\frac{\cos(kR_a)}{kR_a}\left[\frac{1}{kR_a}-\frac{3(z_n-z_m)^2}{kR_a^3}\right]\\&+\frac{\sin(kR_b)}{kR_b}\left[1-\frac{(1+(z_n+z_m)^2k^2)}{k^2R_b^2}+\frac{3(z_n+z_m)^2}{k^2R_b^4}\right]\\&+\frac{\cos(kR_b)}{kR_b}\left[\frac{1}{kR_b}-\frac{3(z_n+z_m)^2}{kR_b^3}\right]\end{aligned}\right\}. \tag{10}$$

Self terms for $R_a=|\bar{r}_m-\bar{r}_n|$ in eq (9), (when $m = n$), are dealt with as a limiting case since direct calculation leads to indeterminate forms. Using a series expansion for the $\frac{\sin(kR_a)}{kR_a}$ terms, the self terms dependent on R_a become $\frac{k}{8\pi\omega\mu_0}\left\{1-\frac{1}{6}\right\}=\frac{k}{8\pi\omega\mu_0}\cdot\frac{5}{6}$.

To determine the closed form for the numerator of eq (1), we take the z-component of the electric field derived in eq (2). Letting $R_m = |\bar{r} - \bar{r}_m|$ and $R'_m = |\bar{r} - \bar{r}'_m|$ results in the following:

$$E_z(\bar{r})_m = \frac{1}{4\pi}\left\{\begin{array}{l}\dfrac{e^{-jkR_m}}{kR_m}\left[1 - \dfrac{j}{kR_m} - \dfrac{(1+(z-z_m)^2k^2}{k^2R_m^2} + \dfrac{3j(z-z_m)^2}{kR_m^3} + \dfrac{3(z-z_m)^2}{k^2R_m^4}\right] \\ + \dfrac{e^{-jkR'_m}}{kR'_m}\left[1 - \dfrac{j}{kR'_m} - \dfrac{(1+(z+z_m)^2k^2}{k^2R_m'^2} + \dfrac{3j(z+z_m)^2}{kR_m'^3} + \dfrac{3(z+z_m)^2}{k^2R_m'^4}\right]\end{array}\right\}. \quad (11)$$

The m subscript on the electric field refers to the element or current source responsible for generating the field, as previously given in eq (7). Calling the numerator matrix A, we can write A as the outer product of two vectors, i.e., $A = \bar{\varepsilon}\bar{\varepsilon}^*$, where $\bar{\varepsilon}$ is column vector and $\bar{\varepsilon}^*$ is the complex conjugate row vector. Using eq (11), the elements of $\bar{\varepsilon}$ are given as

$$\bar{\varepsilon} = \frac{R_{ave}}{\sqrt{2\eta}} E_m(\bar{r}) \text{ and } \bar{\varepsilon}^* = \frac{R_{ave}}{\sqrt{2\eta}} E_m^*(\bar{r}) \ . \quad (12)$$

We want to maximize the ratio $p = \frac{A}{B}$, which equates to finding the largest eigenvalue of

$$A\bar{a} = \lambda_i B\bar{a} \ , \quad (13)$$

where $\bar{a}$ represents a scaling of the current vector. Due to the structure of the matrices A and B, only one nonzero eigenvalue exists for eq (13). We solve for the maximum of this ratio using the following equation

$$\max\{p\} = \lambda_{\max} = \bar{\varepsilon}^* B^{-1} \bar{\varepsilon} \ . \quad (14)$$

In addition, we can determine the magnitude and phase of the necessary current scaling from:

$$\bar{a} = B^{-1}\bar{\varepsilon} \ . \quad (15)$$

Two important points to note are as follows. First, the scaled currents determine the resulting gain at the observation point. Second, the existence of only a single nonzero eigenvalue follows from the theory of eigenvalues and eigenvectors. The zero eigenvalues correspond to eigenvectors orthogonal to the eigenvector associated with the nonzero eigenvalue. Physically, the currents corresponding to the zero eigenvalues produce no field at the observation point [14]. Only the currents associated with the nonzero eigenvalue produce fields at the observation point. A succinct development of eq (13) through eq (15) is found in Reference [15].

The sensitivity of the gain to the current magnitude and phase represents an important part of this analysis. Using the vector $\overline{|a|}$, whose elements are the magnitudes of the optimized currents, the sensitivity of the gain to the optimized current magnitudes follows from

$$D\left(\overline{|a|}\right)=\frac{\overline{|a|}^{*} A \overline{|a|}}{\overline{|a|}^{*} B \overline{|a|}}, \tag{16}$$

where D represents the gain at the particular observation point used in the optimization process. In other words, we simply calculate the gain using only optimized current magnitude information. Similarly, using $\overline{\angle a}$, the sensitivity of the gain to only the phases of the optimized currents follows from

$$D\left(\overline{\angle a}\right)=\frac{\overline{\angle a}^{*} A \overline{\angle a}}{\overline{\angle a}^{*} B \overline{\angle a}}. \tag{17}$$

With the basic theory in place, we now describe an appropriate simulation environment to investigate some key attributes of the proposed approach.

3. Simulation Setup

Figure 2 below includes additional details on the basic simulation configuration introduced in figure 1. Three important features in all of the simulation runs include:

1. ground plane modeled as a PEC, infinite in the x and y directions;
2. z-directed Hertzian dipoles, with current distribution defined in eq (7);
3. observation points chosen in the $z = 1.3$ m plane.

In the simulation setup, the ground plane represents the floor of a room or building. The elements equate to the wireless devices randomly placed throughout the room or building as part of the communication system (hereafter called simply the system). A height of 1.3 m for the observation points approximates the antenna height of the radio device on the emergency response personnel, and the z-directed field corresponds to the vertically polarized orientation of the antenna. Figure 2 provides an example of four elements at a height of 1.3 m over the ground plane.

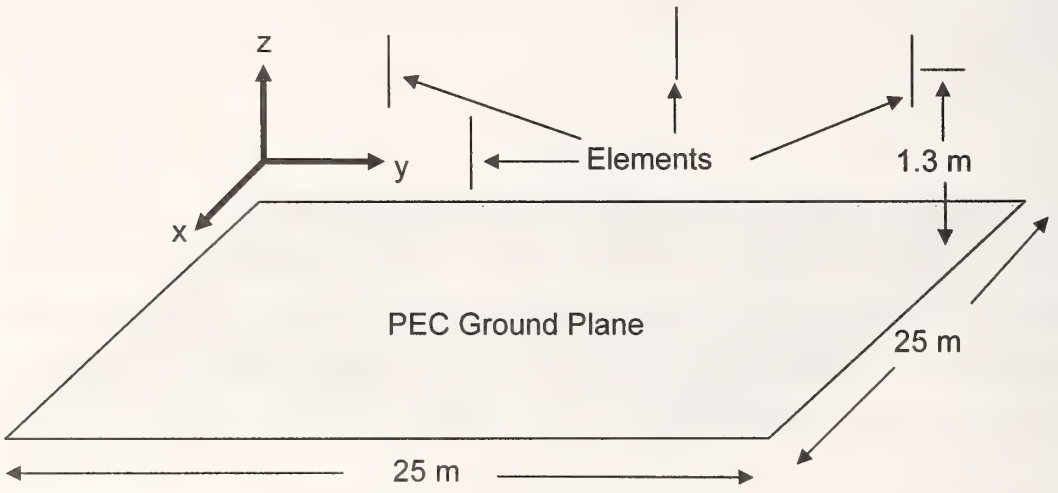

Figure 2. Four z-directed elements above an infinite PEC ground plane. All dipole elements located at a height of $z = 1.3$ m. The footprint of the volume containing the elements is 25 m × 25 m.

Each simulation run focuses on the effect of particular system parameters, which include:

1. radio frequency range of 100 MHz–5.0 GHz;
2. x ,y , and z coordinates for observation points:

a. random x and y coordinates uniformly distributed over a [–8.0 m, 8.0 m] square (see figure 3 below);
b. deterministic locations within the array footprint (see figure 4 below);
c. random x and y coordinates uniformly distributed in a 10 m perimeter around the 25 m array footprint (see figure 5 below);

3. x ,y , and z coordinates for element locations:
   a. random x and y coordinates uniformly distributed over [–12.5 m, 12.5 m] square, height of z = 1.3 m;
   b. random x and y coordinates uniformly distributed over [–12.5 m, 12.5 m] square, uniform random distribution for various ranges of z;
4. number of dipole elements ranging from 2 to 20 elements;
5. sensitivity to optimized current parameters:
   a. magnitude sensitivity calculated from eq (16);
   b. phase sensitivity calculated from eq (17).

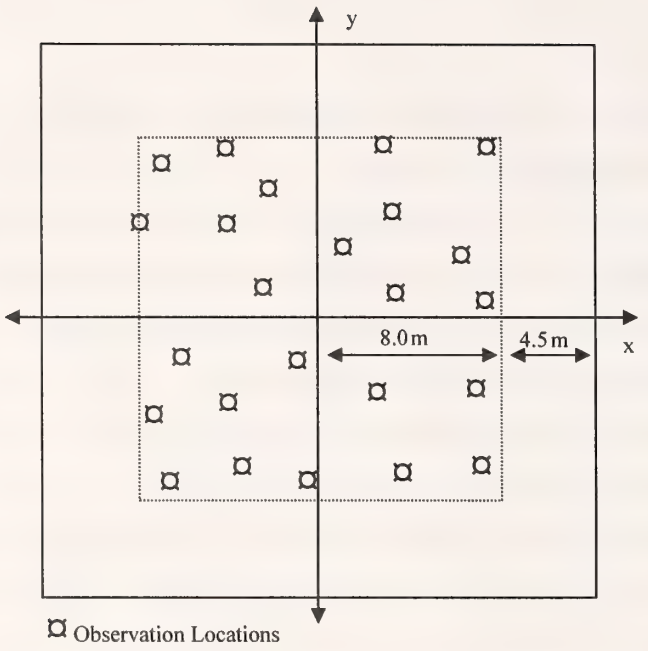

Figure 3. Example of random observation points within the array in the z = 1.3 m plane. Array elements (not shown) are randomly located in either a plane or volume, as indicated in number 3 above.

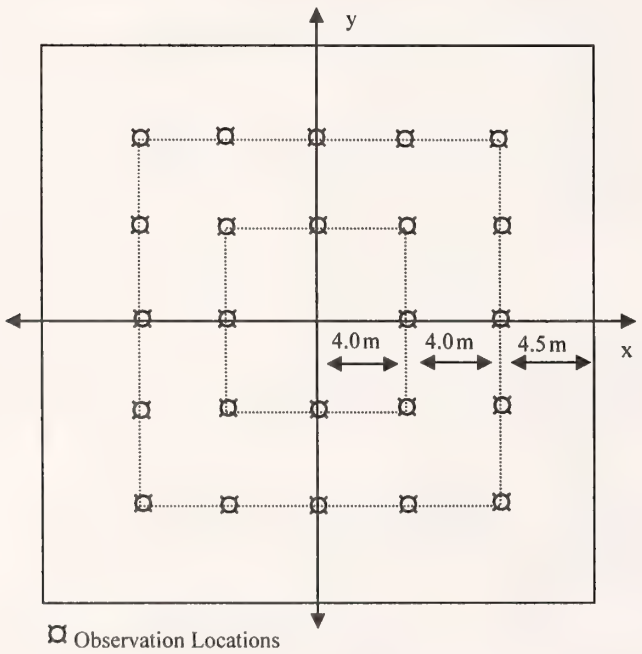

Figure 4. Deterministic observation locations in the z = 1.3 m plane. Array elements (not shown) are randomly located in either a plane or volume, as indicated in number 3.

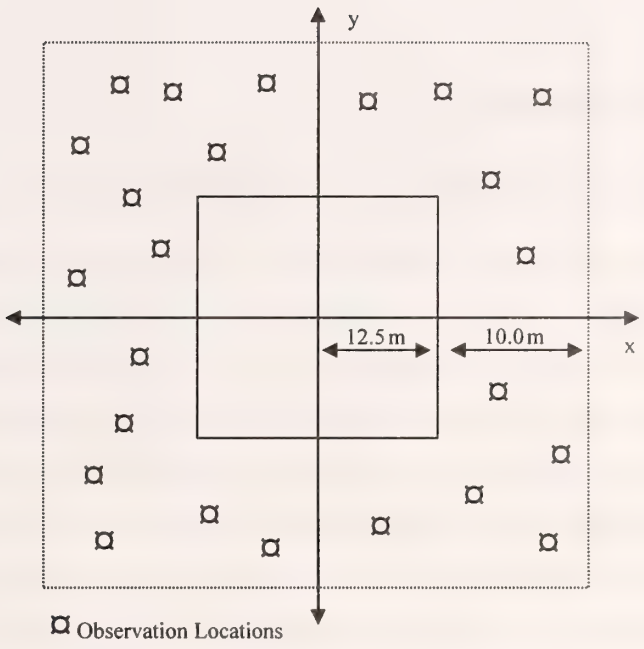

Figure 5. Example of random observation points external to the array elements. Array elements (not shown) are randomly located in either a plane or volume, as indicated in number 3 above.

The simulation environment basically consists of using mathematical software to randomly locate radiating elements and observation points, and then compute the closed form expressions previously discussed in Section 2. Each particular simulation configuration undergoes multiple trials, e.g., 1000 trials with frequency = 100 MHz, observation point x and y coordinates chosen at random, and four dipole elements. Computation of the A and B matrices follows from eq (10) and eq (12), while optimization of the resulting gain is calculated from eq (14). Note in all the simulation runs, the radiating or array elements are located within the notional building volume, whereas the observation points may be either interior or exterior to the building volume, as depicted in the three previous figures. Further details on each set of simulations precede the figures illustrating the corresponding results in Section 4, along with a discussion on each set of figures. Section 5 contains the overall conclusions.

4. Simulation Results

4.1 Average Gain with Elements in a Plane and Interior Observation Points

Each simulation run typically includes 1000 trials, (the only exception is described in Appendix A). A trial consists of first placing the radiating elements in the notional building space, then locating the observation points in accordance with one of the layouts discussed in Section 3, and finally calculating the gain for each observation point by optimizing the current magnitude and phase on each Hertzian dipole element. Thus, each trial generates a number of optimized gains equal to the number of observation points, (usually 24 in these simulations, with the exception described in Appendix A). The average gain is computed by taking the average of the average gain per trial determined at the observation points. A mathematical representation takes the form:

$$D_{ave} = \langle\langle D_i \rangle\rangle = \frac{1}{L}\sum_{L}\left(\frac{1}{l}\sum_{i=1}^{l} D_i\right), \tag{18}$$

where L is the number of trials, l is the number of observation points per trial, D_i is the gain at one observation point, and D_{ave} is the average gain. The $\langle\cdot\rangle$ notation represents the calculation of the average.

Figures 6 to 9 depict simulated gain versus number of elements for five different frequencies, with the number of elements ranging from 2 to 20. Figure 6 shows the average gain calculations based on the x and y coordinates of the observation points uniformly distributed over the interval [–8.0 m, 8.0 m], (figure 3 depicts an example distribution). Figure 7 shows similar simulation results, but with the deterministic observation points chosen to follow the layout presented previously in figure 4. Figures 8 and 9 show the standard deviation corresponding to the average gain of figures 6 and 7, respectively. This represents the standard deviation in the average gain per trial as given by the equation

$$\sigma = \sqrt{\left\langle \left\langle D_{ave} \right\rangle^2 \right\rangle - \left\langle \left\langle D_{ave} \right\rangle \right\rangle^2}\,, \tag{19}$$

where σ is the standard deviation. Based on this series of plots, the method of selecting x and y observation coordinates, such as random versus periodic, in a specific plane of observation does not appear to significantly influence the statistical behavior of the optimization process.

Figures 6 through 9 provide three general insights. First, the average gain increases as the number of elements increases. The gain increases approximately 3 dB when increasing from 4 to 8 elements or from 8 to 16 elements; or in general, a doubling of the elements causes a 3 dB increase in gain. This is not an obvious conclusion since the ratio under consideration as given by eq (1), normalizes the gain by the total system input power. (Note that gain does not simply result from an increasing number of elements; compare to the results in figures 12, 14, and 19.) Second, the standard deviation appears to settle below 0.75 dB in almost all cases. The anomaly for the 100 MHz behavior in figures 8 and 9 is still under investigation, but we note that the same behavior occurs for both the random and deterministic observation locations.

The third insight arises when we examine the behavior due to the electrical height of the elements above the ground plane. Nearly identical plots of the average gain occur for the frequencies of 1.0 GHz, 2.5 GHz, and 5.0 GHz in all four of the figures. However, the 100 MHz plot indicates approximately an improvement of 1 dB over these three frequencies and a 2 dB improvement over the 500 MHz case, for all numbers of elements. This result is due to the height over the PEC ground plane relative to a wavelength at a specific frequency resulting in constructive or destructive interference. The use of the PEC in the simulations represents a crude approximation to the real world surface, such as a concrete floor, so these differences due to height may be less pronounced in the implementation of a system. However, since the actual implementation can be expected to have devices located less than 2 m above the ground, the choice of frequencies could significantly impact the actual gain achieved.

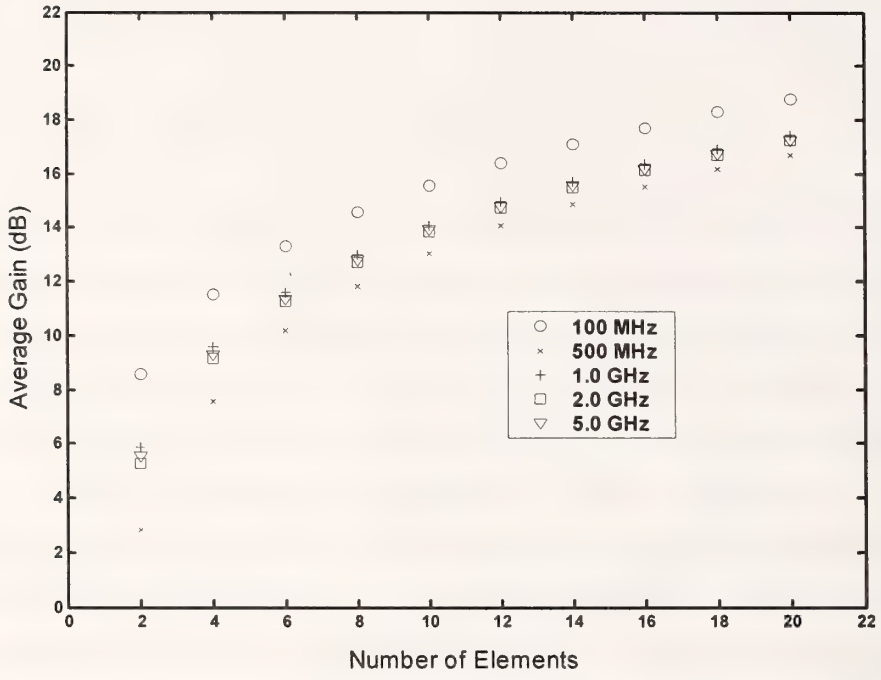

Figure 6. Average gain using 1000 trials and 24 random observation positions over 16 m × 16 m square area.

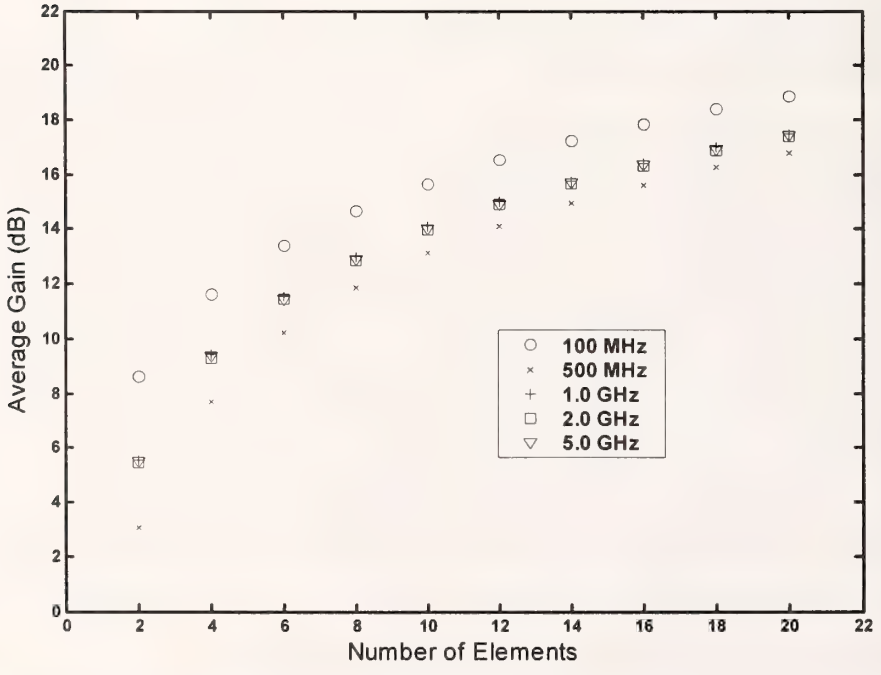

Figure 7. Average gain using 1000 trials and 24 deterministic observation positions of figure 4.

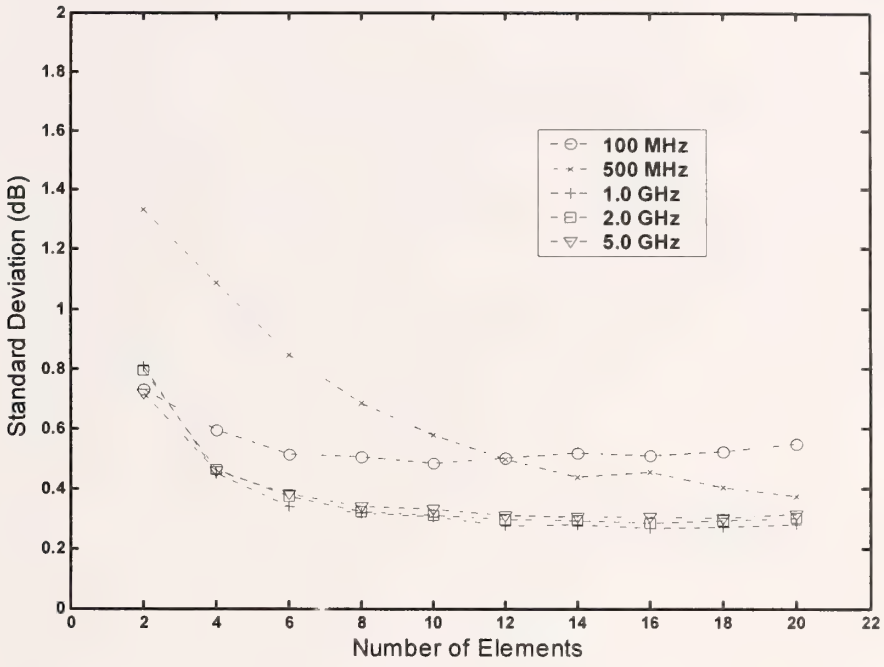

Figure 8. Standard deviation of average gain plotted in figure 6.

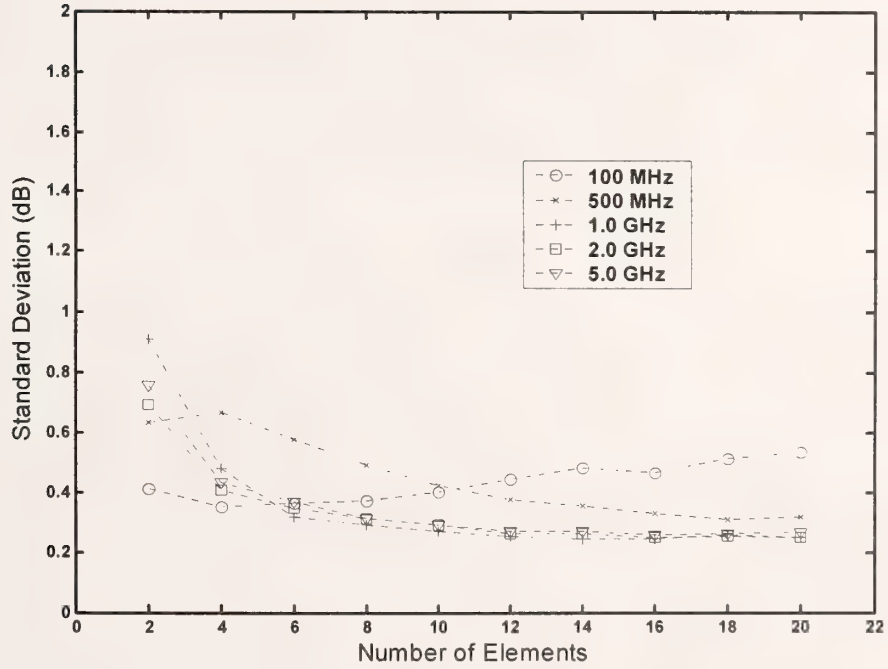

Figure 9. Standard deviation of average gain plotted in figure 7.

4.2 Effect of Current Magnitude on Optimized Gain

Figures 10 through 12 illustrate the effects of using only the optimized current magnitudes in computing the gain results. Figures 10 and 11 result from taking only the magnitude of the optimized current vector for the same configurations used to generate figures 6 and 7. After determining the optimized current scaling from eq (15), application of eq (16) provides the gain using only the optimized current magnitudes. All the elements are excited in phase, i.e., with a zero phase difference between elements.

As anticipated from the previous results, figures 10 and 11 exhibit no significant differences. However, the overall gain is substantially decreased from the gain depicted in figures 6 and 7. For instance, for 10 elements in figures 6 and 7, all frequencies exhibit a gain in excess of 12 dB, while for 10 elements all frequencies are below 8 dB in both figures 10 and 11. Also, the rate of gain increase, approximately 1 dB per doubling of elements in figures 10 and 11, represents a substantial decrease from the 3 dB per doubling of elements depicted in figures 6 and 7.

Figure 12 illustrates an important result because it provides a baseline with which to compare current optimization techniques. For comparison purposes, a random uniform distribution for the current magnitudes with identical phases is used in place of the optimized current scaling vector in eq (16). The gain is computed from

$$D(\bar{a}) = \frac{\bar{a}^* A \bar{a}}{\bar{a}^* B \bar{a}}, \tag{20}$$

where $\bar{a}$ is a vector with a uniform random distribution for current magnitudes and zero phase. The results are shown in figure 12, where the gain remains fairly constant as the number of elements increases. The gain in figures 10 and 11 exceeds the gain in figure 12 for all five frequencies and number of elements. This indicates the optimized current magnitude information alone provides gain, even though the amount of gain may be substantially reduced.

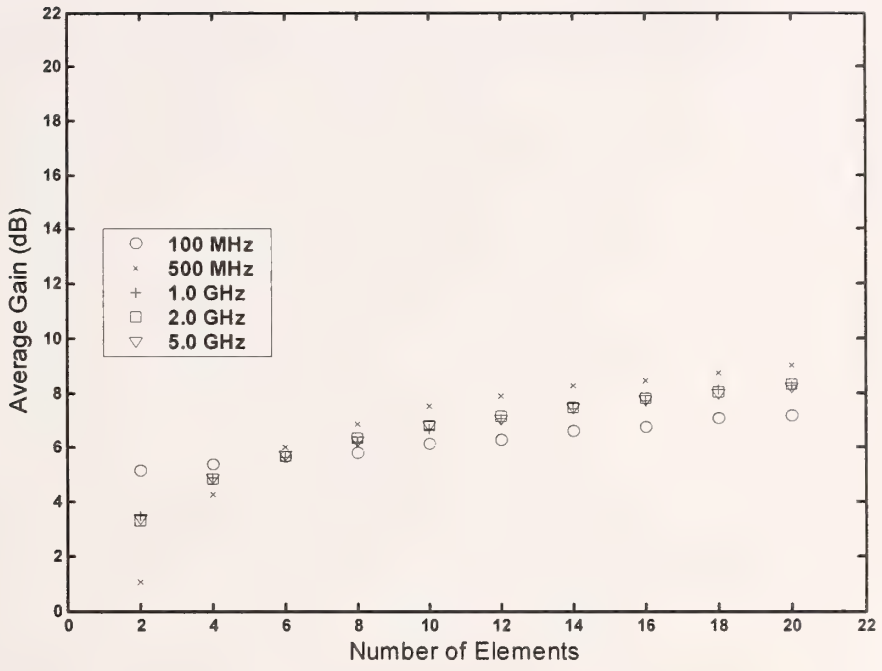

Figure 10. Average gain using only the magnitude of the optimized currents for 1000 trials and 24 random positions over 16 m × 16 m square area in the z = 1.3 m plane.

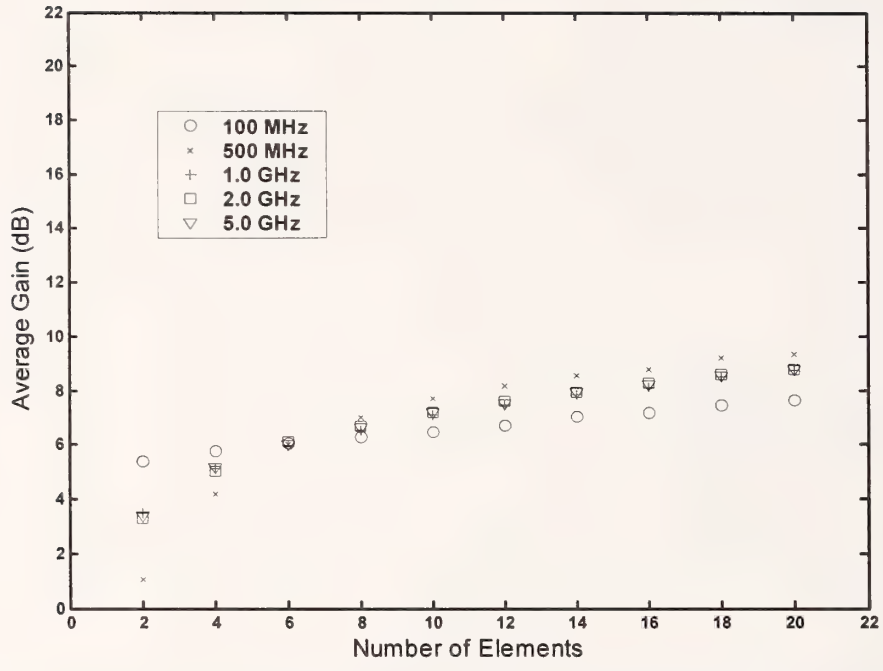

Figure 11. Average gain using only the magnitude of the optimized currents for 1000 trials and 24 deterministic positions of figure 4.

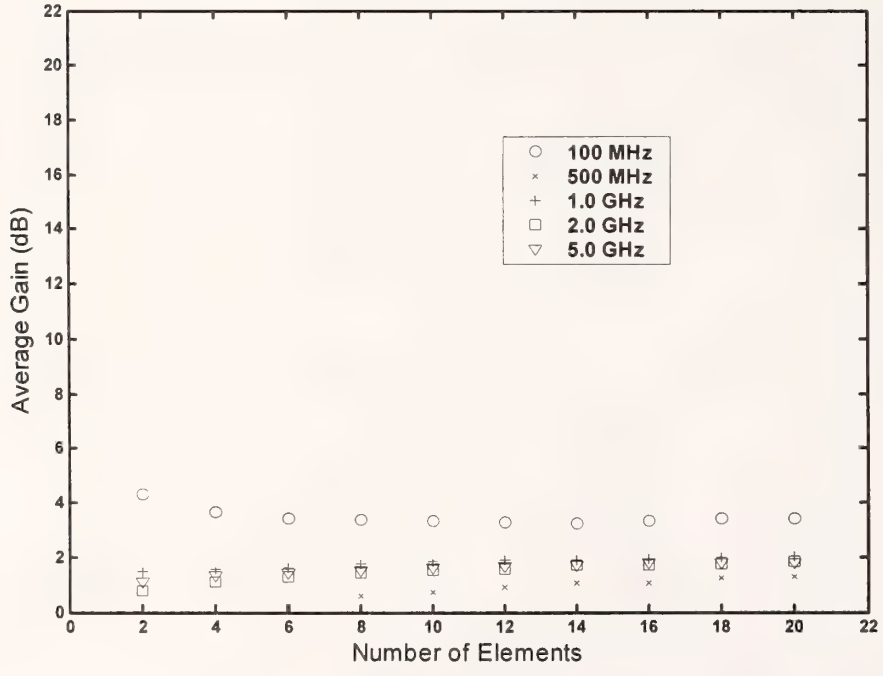

Figure 12. Average gain using uniformly distributed random current magnitudes and identical phase for 1000 trials and 24 random positions over 16 m × 16 m square area in the z=1.3 m plane.

4.3 Effect of Current Phase on Optimized Gain

The next two figures illustrate the effect of optimized phase on the gain. Figure 13 illustrates the gain obtained from using only the optimized phase information from eq (15) with random observation points. This figure uses the same points as the average gain plots in figures 6 and 10. These results demonstrate the significant effect of phase in achieving the maximum possible gain for a given configuration. In comparing the gain results achieved using optimized current phase information only versus optimized current magnitude information only, figure 13 versus figure 10 indicates a higher average rate of increase in gain. For example, at 100 MHz, the rate of increase in gain is approximately 2 dB per doubling of the elements when using the optimized current phase information (see figure 13), as compared to approximately 1 dB per doubling of the elements when using the optimized magnitude information (see figure 10).

Finally, figure 14 shows the results of using a uniform random distribution for the phase with unity magnitude for the current vector, $\overline{a}$, in eq (20). The use of unity magnitude currents with uniformly distributed random phases over [0, 2π] depicted in figure 14 is nearly identical to the results depicted in figure 12. Figures 12 and 14 show that the optimization and/or control of the excitation currents (either current phase or magnitude), is required to achieve gain at a given observation point.

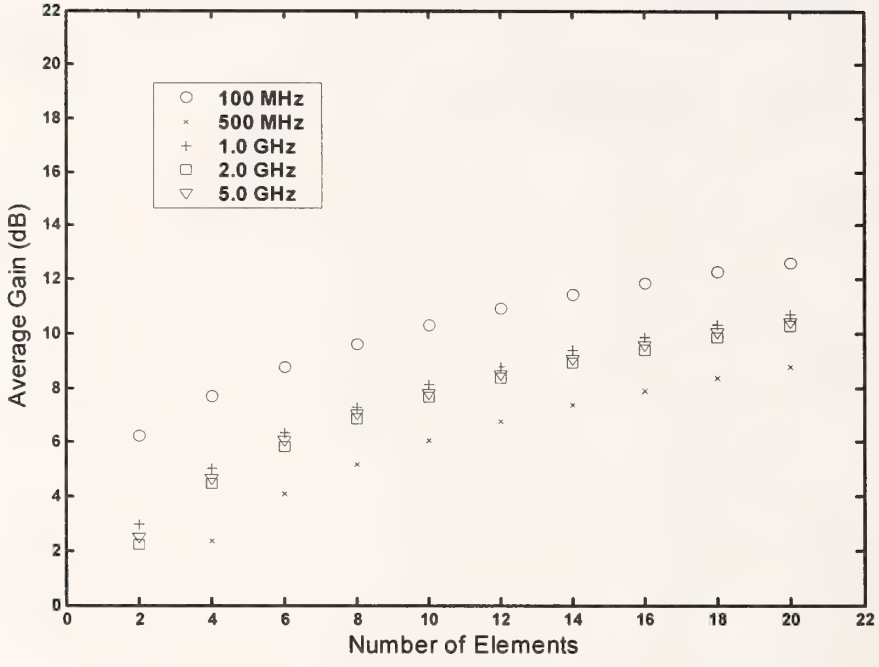

Figure 13. Average gain using only phase of optimized currents for 1000 trials and 24 random positions over 16 m × 16 m square in the z = 1.3 m plane.

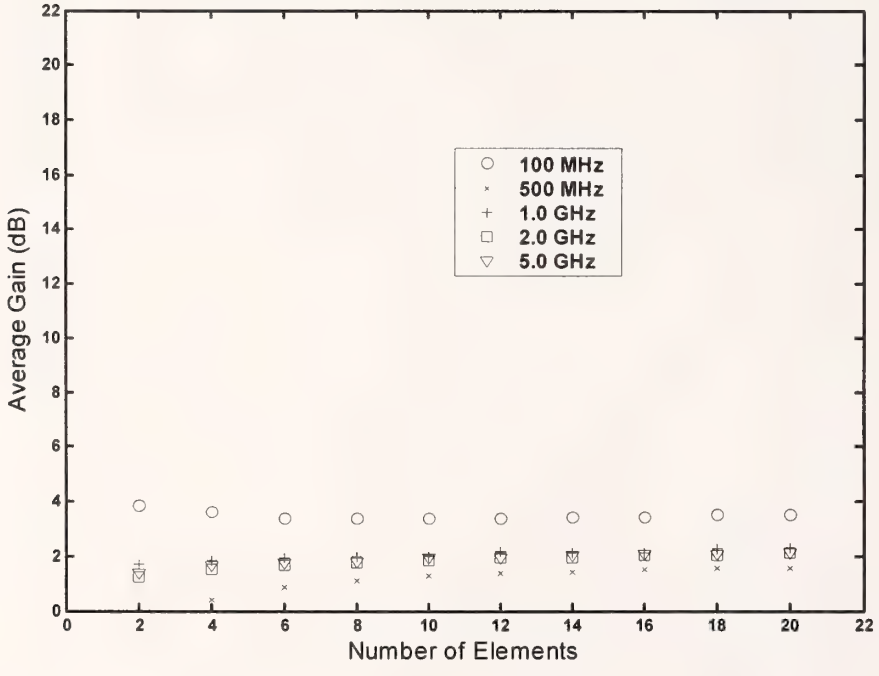

Figure 14. Average gain using uniformly distributed random phase with unity magnitude currents for 1000 trials and 24 random positions over 16 m × 16 m square area in the z = 1.3 m plane.

4.4. Average Gain with Elements in a Plane and Exterior Observation Points

Communication into a building can also be difficult, so the next results focus on the possible improvement in gain using this multiple element system and optimization process when the observation point lies within a 10 m perimeter of the building. Figure 5 illustrates an example distribution of the observation points. Figures 15 and 16 depict the average gain and corresponding standard deviation for the case where the observation point lies in a 10 m perimeter of the array boundary. The rate of gain increase in Figure 15 indicates a gain of approximately 3 dB per doubling of the number of elements, which matches the gain per element increase exhibited in figures 6 and 7. The general trend in the standard deviations plotted in Figure 16 also mimics the trend shown in figures 8 and 9 (although σ is higher for some specific cases).

Figures 17 and 18 show gain results based on only the optimized current magnitudes and phases, respectively. Figure 19 depicts the use of unity magnitude current with uniformly distributed random phases over $[0, 2\pi]$ in calculating the gain. (The case of uniform random current magnitudes with equal phases is effectively the same as the results in figure 19, and thus omitted.) While using either the optimized current magnitudes or phases provides a gain increase over the random current case, the optimized phases enable a larger increase. The rate of increase using the optimized phases tracks the rate of approximately 2 dB per doubling of the elements when using the interior observation points. However, the optimized magnitudes begin to flatten out for the 14-element configuration.

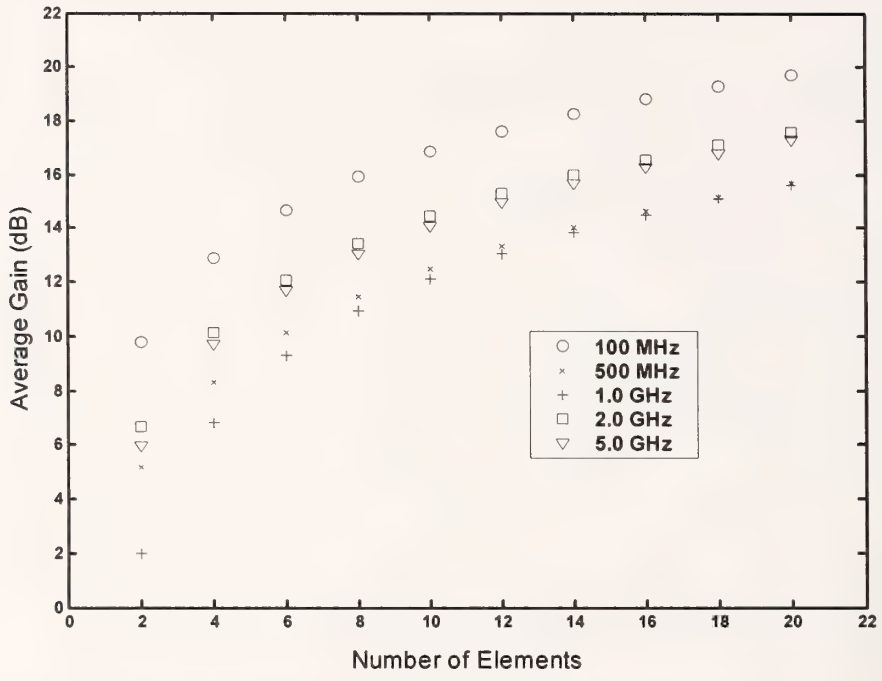

Figure 15. Average gain for 1000 trials of 24 random observation points in the 10 m perimeter of the array.

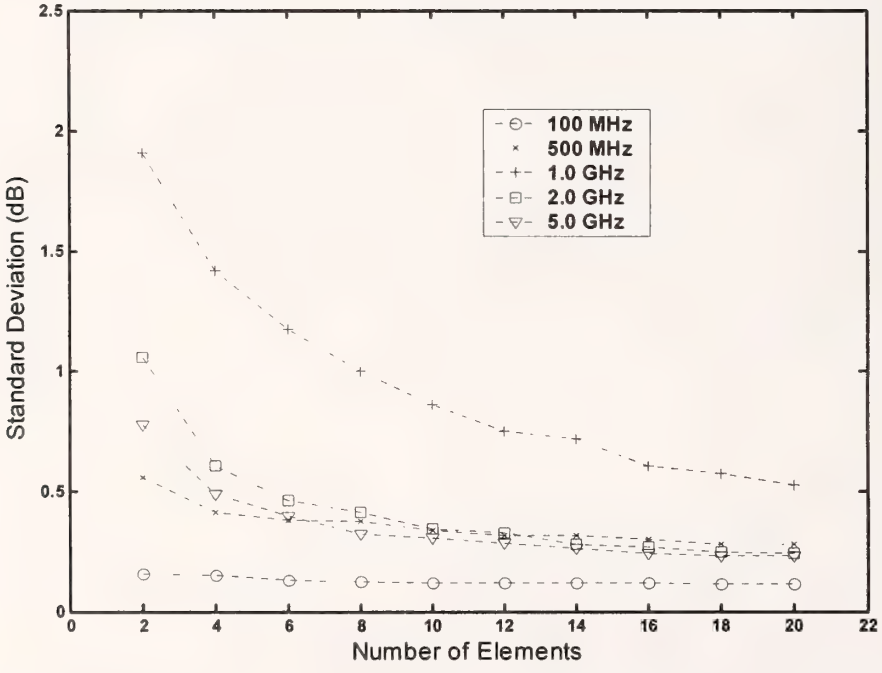

Figure 16. Standard deviation of average gain for 1000 trials of 24 random observation points in the 10 m perimeter of the array.

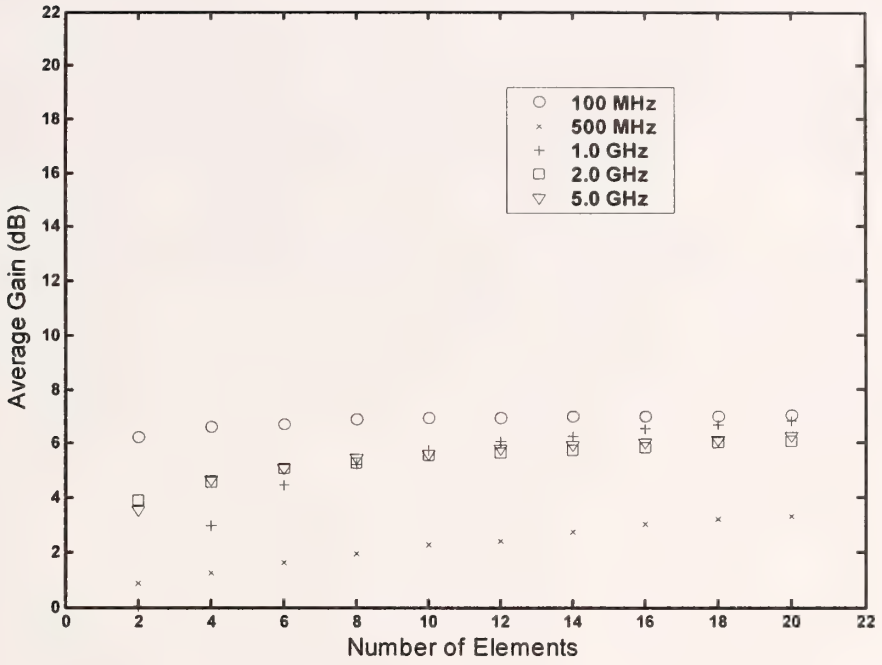

Figure 17. Average gain using only the magnitudes of the optimized currents for 1000 trials and 24 random observation points in the 10 m perimeter of the array.

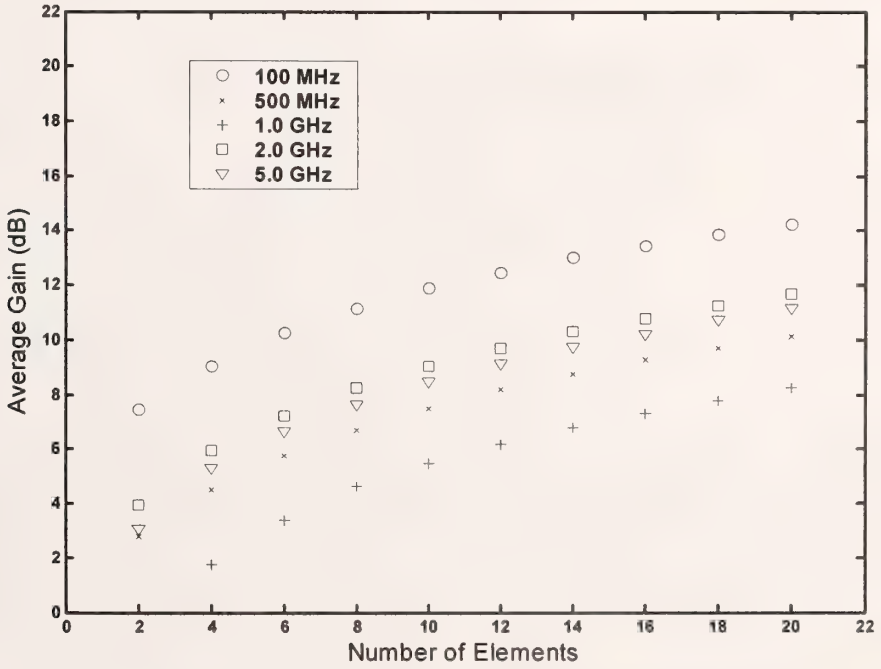

Figure 18. Average gain using only the phase of the optimized currents for 1000 trials and 24 random observation points in the 10 m perimeter of the array.

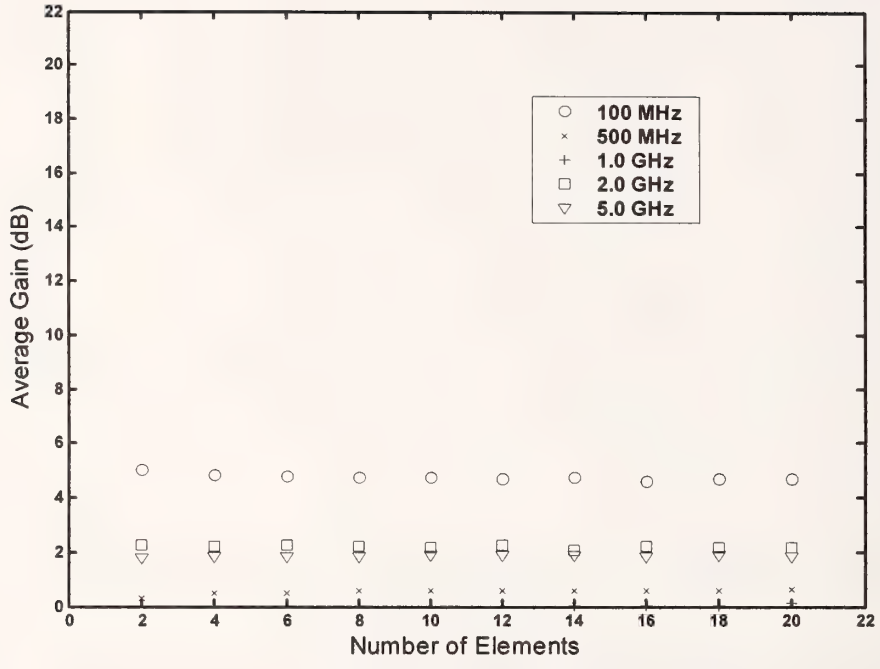

Figure 19. Average gain using uniformly distributed random phase with unity magnitude currents for 1000 trials and 24 random observation points in the 10 m perimeter of the array.

4.5 Effect of Elements Located in a Volume versus a Plane

This next series of plots (figures 20 through 31), depicts the gain behavior when the radiating elements are not constrained to the same plane as the observation point. Specifically, coordinates of the radiating elements are uniformly distributed along the three coordinate axes, x, y, and z, while the observation points all lie in the z = 1.3 m plane. The first six plots illustrate the gain and standard deviation for three different volumes with observation points within the building boundaries, while the next six plots result from observation points in the 10 m perimeter. In all six cases (three each for the interior and exterior observation points), the x and y coordinates of the elements are random uniformly distributed in the interval [–12.5 m, 12.5 m]. The z coordinates are random uniformly distributed as well, over one of the three possible intervals,

[0.1 m, 0.5 m], [0.1 m, 1.0 m], or [0.1 m, 1.5 m]. Note, these volume intervals start at z = 0.1 m in anticipation of the elements being some finite height above the ground in a practical system.

In the first three plots (figures 20, 21, and 22), the average gain does not change significantly as the volume of possible element locations is increased. Also, the gain exhibits the same rate of increase as when the elements all lie in the z = 1.3 m plane, giving approximately 3 dB per doubling of the elements (compare to figures 6 and 7).

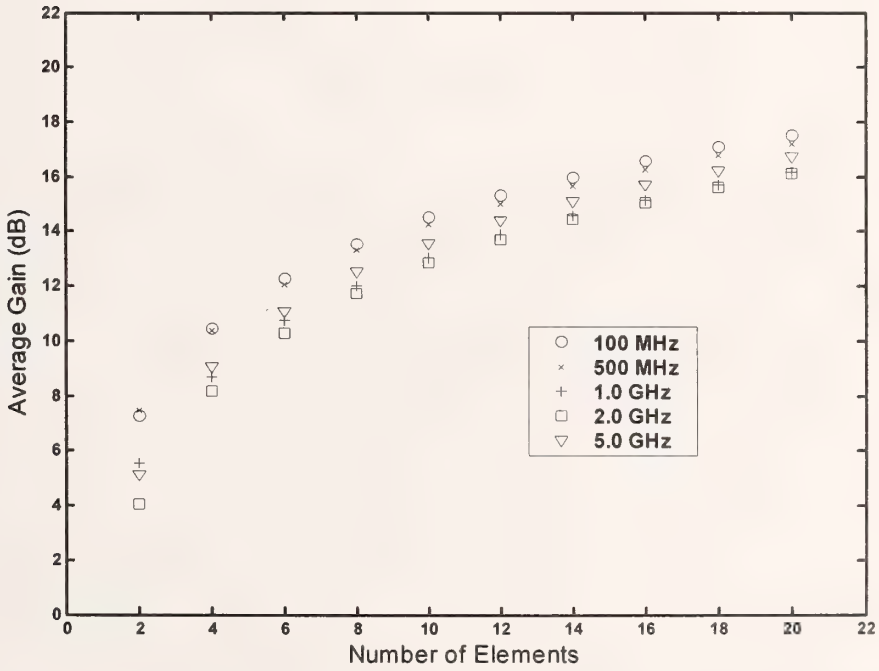

Figure 20. Average gain using 1000 trials and 24 random observation positions over 16 m × 16 m square area; random radiating elements in a volume 25 m × 25 m × 0.4 m; z positions range over the interval [0.1 m, 0.5 m].

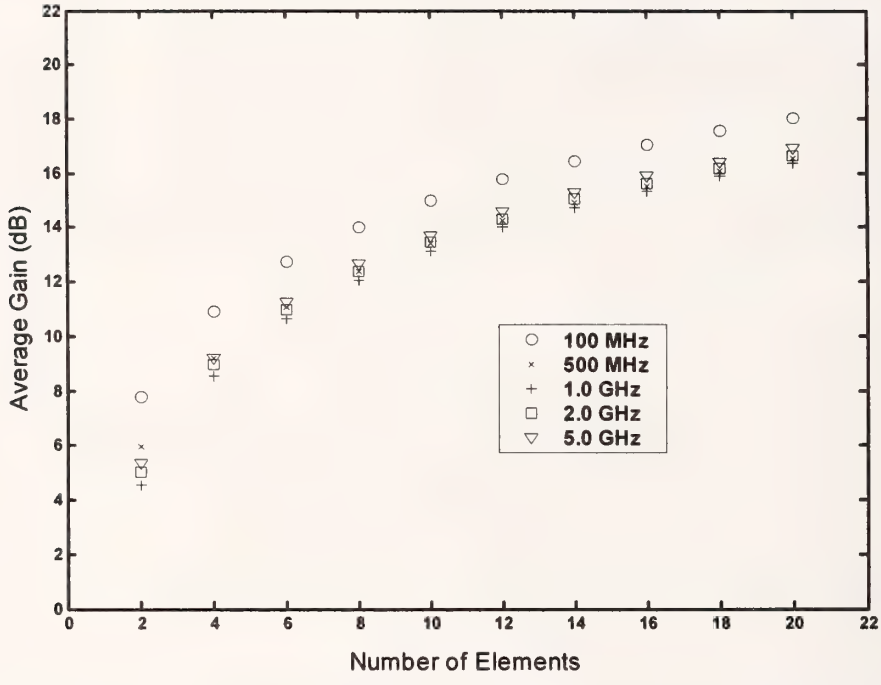

Figure 21. Average gain using 1000 trials and 24 random observation positions over 16 m × 16 m square area; random radiating elements in a volume 25 m × 25 m × 0.9 m; z positions range over the interval [0.1 m, 1.0 m].

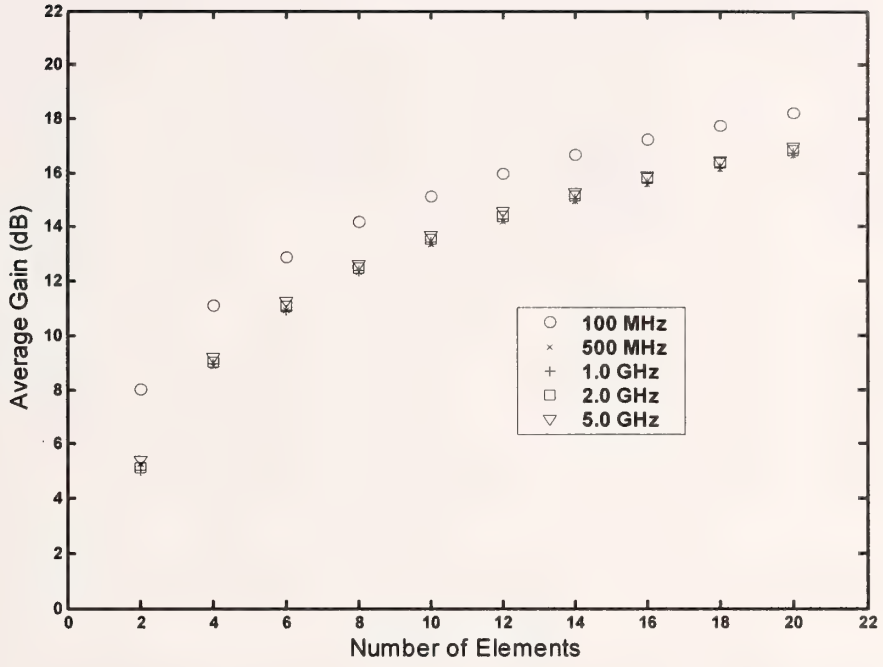

Figure 22. Average gain using 1000 trials and 24 random observation positions over 16 m × 16 m square area; random radiation elements in a volume 25 m × 25 m × 1.4 m; z positions range over the interval [0.1 m, 1.5 m].

These next three plots (figures 23, 24, and 25), illustrate the standard deviation associated with the three previous gain plots. In all three case, the standard deviation falls below 1 dB for all frequencies after only six elements. Placing the elements in a volume, as opposed to a single plane appears to smooth the standard deviation. The combination of the gain and standard deviation indicate an overall smoothing effect from allowing the elements to reside at a variety of heights. An actual system will likely utilize elements at a variety of heights, so this smoothing behavior without sacrificing gain represents an added benefit.

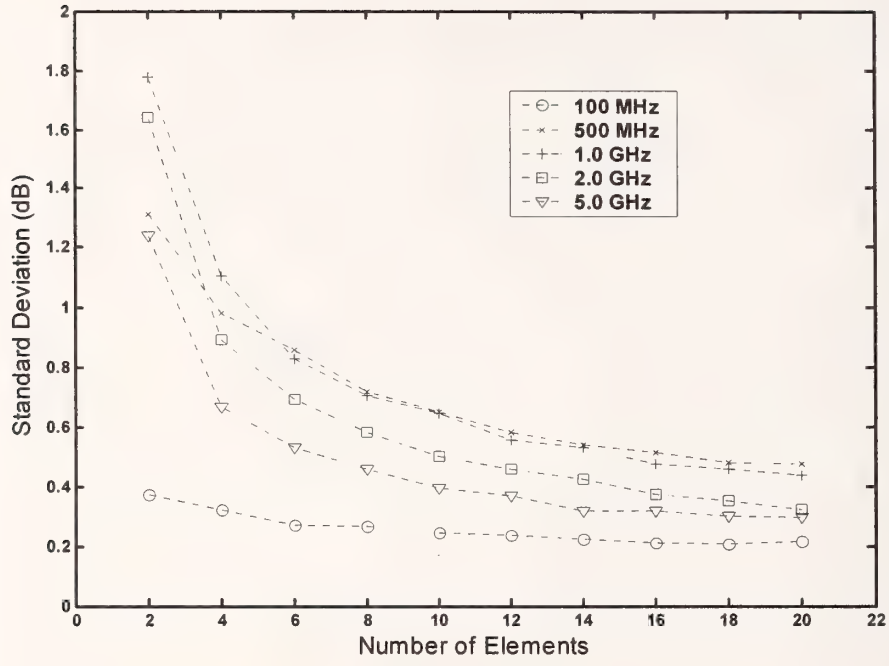

Figure 23. Standard deviation of average gain results shown in figure 20.

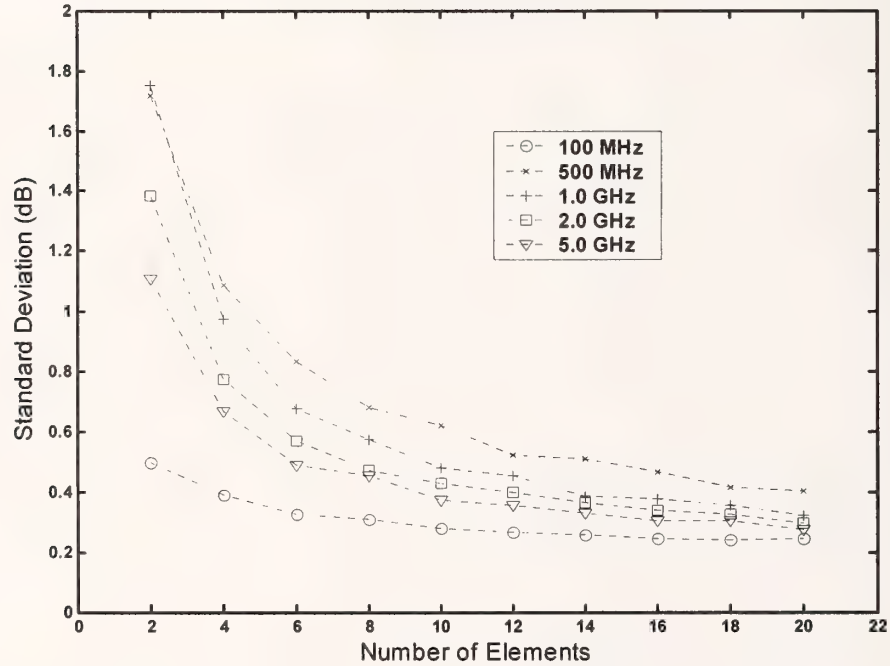

Figure 24. Standard deviation of average gain results shown in figure 21.

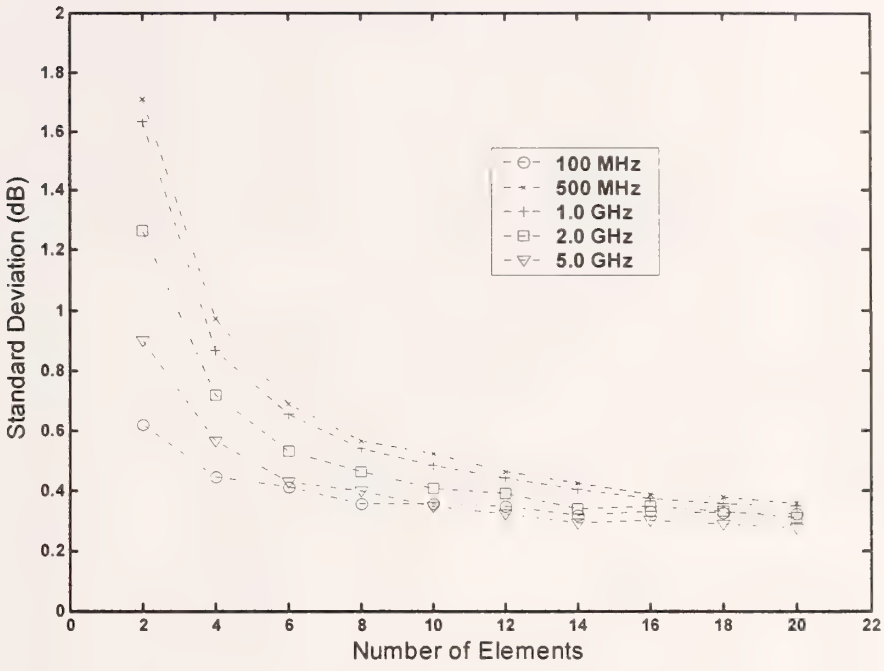

Figure 25. Standard deviation of average gain results shown in figure 22.

The next series of plots (figures 26, 27, and 28), shows the average gain and the corresponding standard deviation when the observation point resides in the 10 m perimeter of the element volume. All the observation points lie in the z = 1.3 m plane and are randomly distributed. The behavior is very similar to the case with interior observation points, namely a smoothing effect on the standard deviation while still maintaining the same rate of gain increase as when the elements all reside in the z = 1.3 m plane. The spread of the average gain between frequencies decreases from approximately 6 dB in the planar case to less than 4 dB in the volume case. As mentioned for the previous six plots, this indicates a potential added benefit for an actual system.

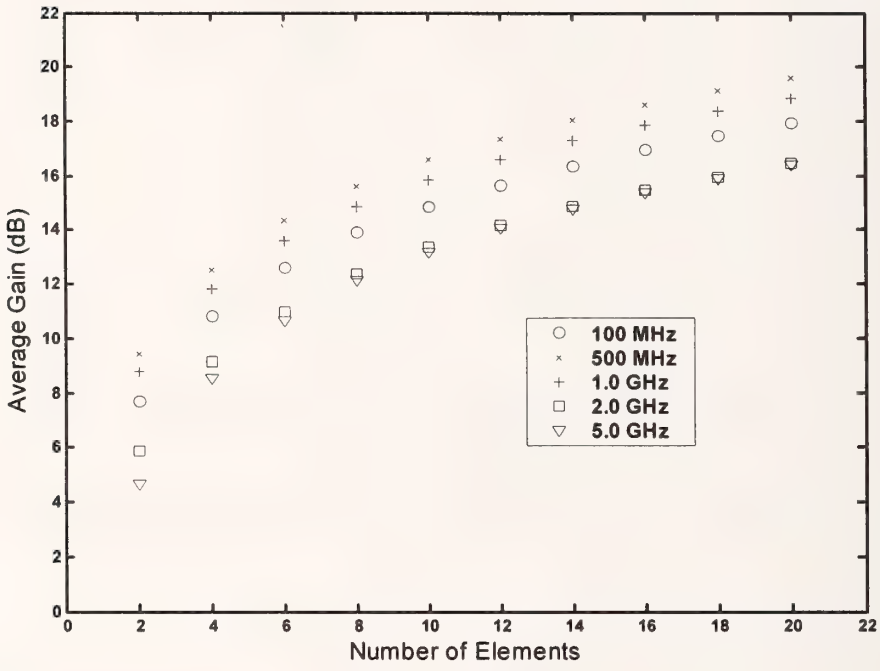

Figure 26. Average gain using 1000 trials and 24 random observation positions over 10 m perimeter; random radiating elements in a volume 25 m × 25 m × 0.4 m; z positions range over the interval [0.1 m, 0.5 m].

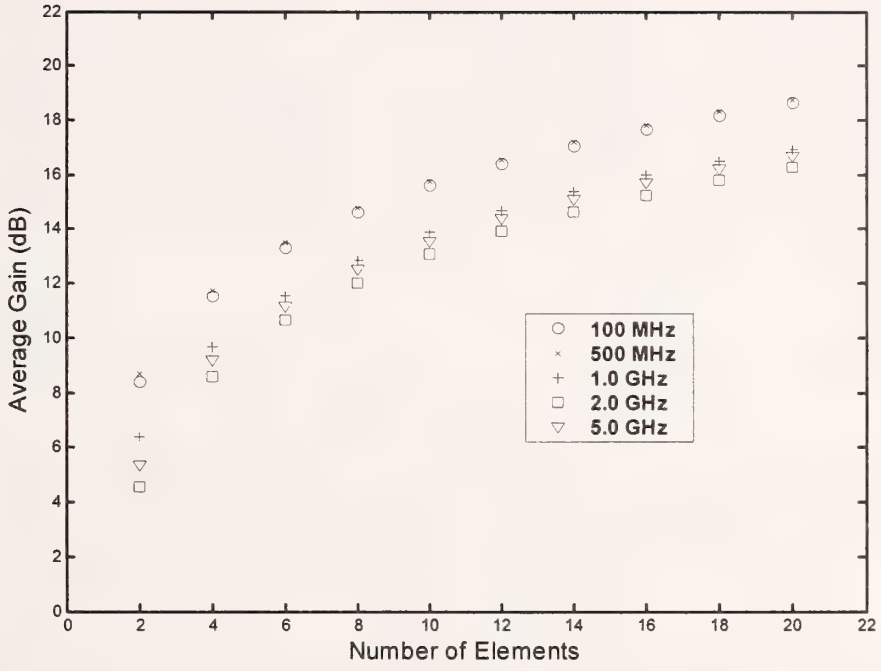

Figure 27. Average gain using 1000 trials and 24 random observation positions over 10 m perimeter; random radiating elements in a volume 25 m × 25 m × 0.9 m; z positions range over the interval [0.1 m, 1.0 m].

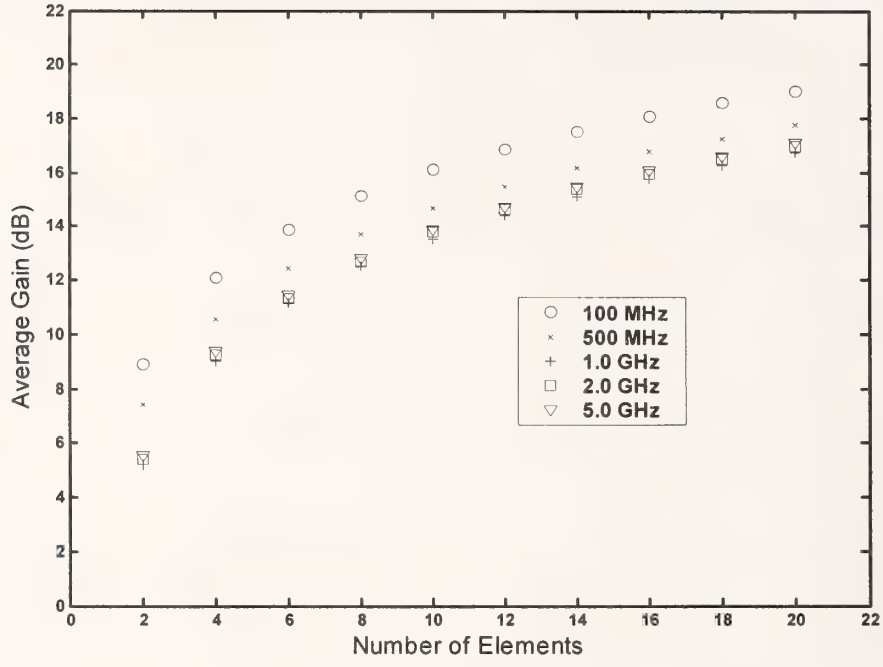

Figure 28. Average gain using 1000 trials and 24 random observation positions over 10 m perimeter random radiation elements in a volume 25 m × 25 m × 1.4 m; z positions range over the interval [0.1 m, 1.5 m].

These next three plots (figures 29, 30, and 31), illustrate the standard deviation associated with the three previous gain plots. In all three plots, the standard deviation drops below 1 dB for greater than four elements. The spread between frequencies is slightly greater than when the observation points reside on the interior of the building, but the difference is not large.

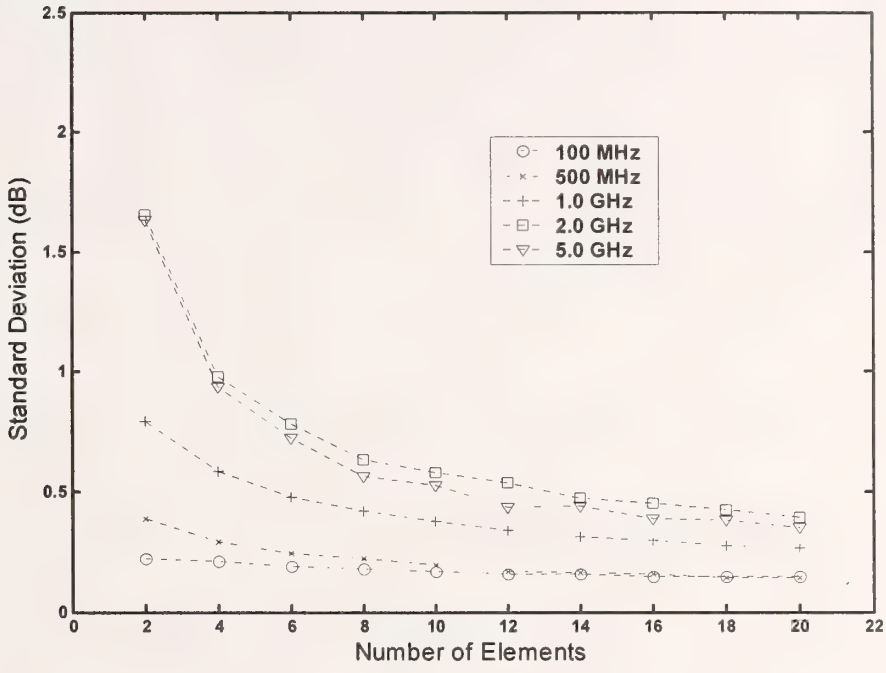

Figure 29. Standard deviation of average gain results shown in figure 26.

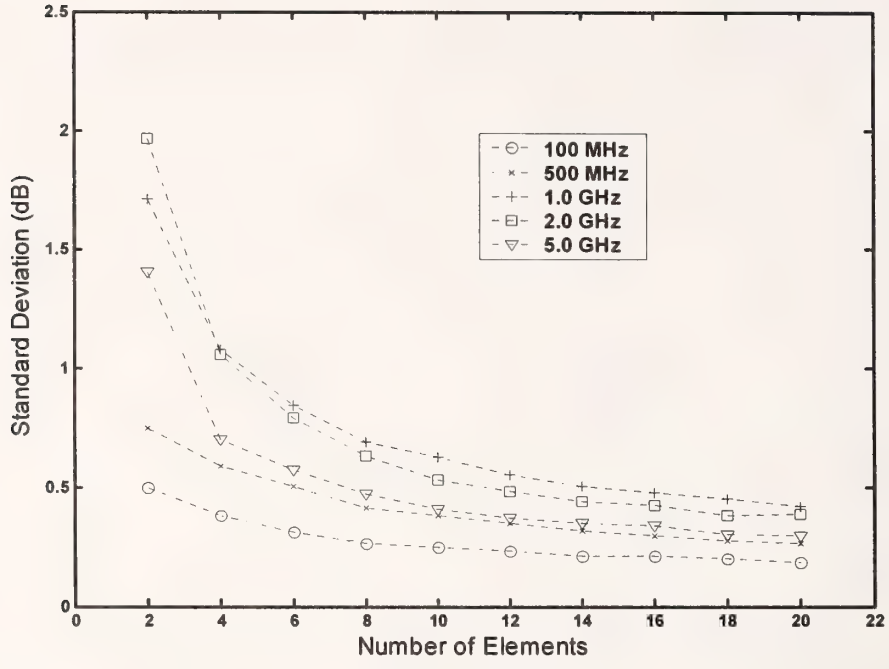

Figure 30. Standard deviation of average gain results shown in figure 27.

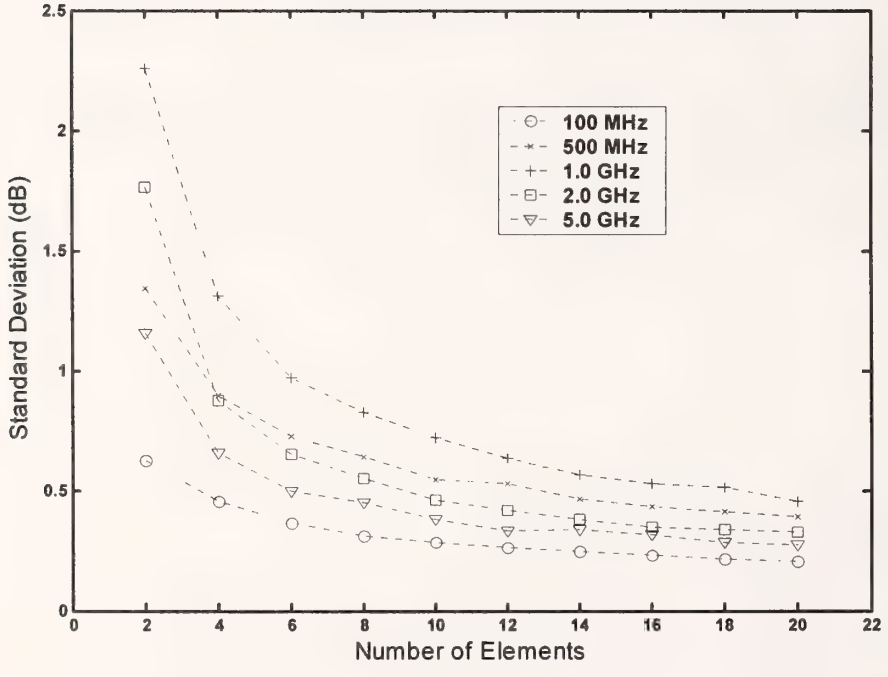

Figure 31. Standard deviation of average gain results shown in figure 28.

5. Conclusions and Future Work

Several preliminary conclusions related to communication systems for emergency responders may be drawn from these initial analytic and simulation results.

- An appropriately controlled system of wireless devices can theoretically increase the communication capability within a building by effectively functioning as an antenna array to support optimized directivity of the electromagnetic radiation. This can improve the probability of receiving a radio-frequency signal, as well as the quality of the signal in terms of signal-to-noise ratio.
- The emergency responder can move throughout the building and surrounding area, and receive a similar benefit from the array.
- The average gain increases by approximately 3 dB per doubling of the elements when using optimized current magnitudes and phases. In addition, the overall average gain is greater than 14 dB, with a standard deviation of less than 0.75 dB for all cases involving 20 elements.
- The use of the optimized current phase information only provides approximately 2 dB of gain increase per doubling of the elements. On the other hand, using only the optimized magnitudes provides 1 dB or less of gain per doubling of the number of radiating elements. This implies the achievable gain is affected more by the accuracy of the optimized phases than the optimized magnitudes.
- Placing the elements in a volume versus a single plane may actually benefit a system utilizing several frequencies by smoothing out the gain statistics.

One of the challenges of implementing a system based on this optimization process is the control of the relative phase between elements. An important ongoing investigation examines the effect on gain as the phases deviate from the optimal case. As noted in the fourth bullet above, gain is still achieved when only the optimized current magnitudes are

used, so even if the phase cannot be tightly controlled, gain should be achievable since the current magnitude is fairly straightforward to control.

These preliminary results are encouraging, but further refinement of the simulation environment is necessary. One improvement currently under investigation is the modeling of the ground plane as other than a PEC. Another point of investigation is the effect of mutual coupling between radiating elements. Location sensitivity analysis will help determine how often the optimization process would require updating in reaction to changes in the topology of the system of wireless devices. Finally, the impact of losing some of the array elements must be studied, as the actual practical implementation will operate in a harsh environment.

6. References

[1] E. K. Krupitskii, On the Maximum Directivity of Antennas Consisting of Discrete Radiators. Technical Physics, Vol. 7, No. 3, pp 257-259, September 1962.

[2] J. L. Synge, Directivity for Scalar Radiation. Quarterly of Applied Mathematics, Vol. 24, No. 1, pp. 90-92, 1966.

[3] L. Susman and W. K. Kahn, Measures of Beam Concentration for Scalar Radiation. Radio Science, Vol, 5, No. 7, pp. 1091-1097, July 1970.

[4] R. F. Harrington, Field Computation by Moment Methods. The Macmillan Company, New York, pp. 189-212, 1968.

[5] T.S. Angell and A. Kirsch, Optimization Methods in Electromagnetic Radiation. Springer-Verlag New York, Inc., New York, 2004.

[6] Y. T. Lo, A Probabilistic Approach to Large Aperiodic Antenna Arrays. Proceedings of the Application Forum on Antenna Research, pp. 580-610, January 1964.

[7] Y. S. Shifrin, Statistical Antenna Theory. The Golem Press, Boulder, CO, 1971.

[8] Y.T. Lo and S.W. Lee, Editors, Antenna Handbook: Theory, Applications, and Design. Van Nostrand Reinhold Co. Inc., New York, NY, Chapter 14, 1988.

[9] W. J. L. Queiroz and M.S. Alencar, Project of Antenna Arrays with Random Parameters. Proceedings Brazilian Microwave and Optoelectronics Society/Microwave Theory and Techniques Society, International Microwave and Optoelectronics Conference 2003, pp. 33-38.

[10] F. Tseng and D. K. Cheng, Gain Optimization for Arbitrary Antenna Arrays Subject to Random Fluctuations. IEEE Transactions of Antennas and Propagation, Vol. AP-15, No. 3, pp. 356-366, May 1967.

[11] E. N. Gilbert and S. P. Morgan, Optimum Design of Directive Antenna Arrays Subject to Random Variations. The Bell System Technical Journal, Vol. 34, pp. 637-663, May 1955.

[12] T.S. Angell and A. Kirsch, Optimization Methods in Electromagnetic Radiation. pp. 106-107, 2004.

[13] C. A. Balanis, Antenna Theory: Analysis and Design. John Wiley & Sons, Inc., p. 39, 1997.

[14] R. F. Harrington, Field Computation by Moment Methods. Macmillan, New York. pp. 197-198, 1968.

[15] D.K. Cheng and F.I. Tseng, Gain Optimization for Arbitrary Antenna Arrays. IEEE Transactions on Antennas and Propagation, Communications, pp 973-974, 1965.

Appendix A: Examination of Statistics Gathering Method

This series of plots demonstrates the effect of choosing 1000 observation points and 24 trials versus 24 observation points and 1000 trials. Figures A-1 and A-2 depict the average optimized gain (i.e., using optimized magnitude and phase for element currents to achieve gain at a specific observation point, as performed in Section 4.1), when the observation points reside in the interior and the exterior of the building, respectively. A uniform random distribution on both the x- and y-axis, and the z = 1.3 m plane provide the observation point coordinates. Compare these first two plots to figures 7 and 15, respectively. The results are nearly identical between figure A-1 and figure 7, and figure 15 and figure A-2.

Figures A-3 and A-4 illustrate the corresponding standard deviation of the average gain in figures A-1 and A-2. These two plots compare to figures 9 and 16. All the trends are similar, including the frequency, which shows the greatest standard deviation, namely 500 MHz for figures 34 and 9, and 1.0 GHz for figures A-3 and 16. Since computing the standard deviation of the average per trial generates these plots, some differences are expected. However, statistically, the results are almost identical, which implies either method of collecting first-order statistics will provide similar results.

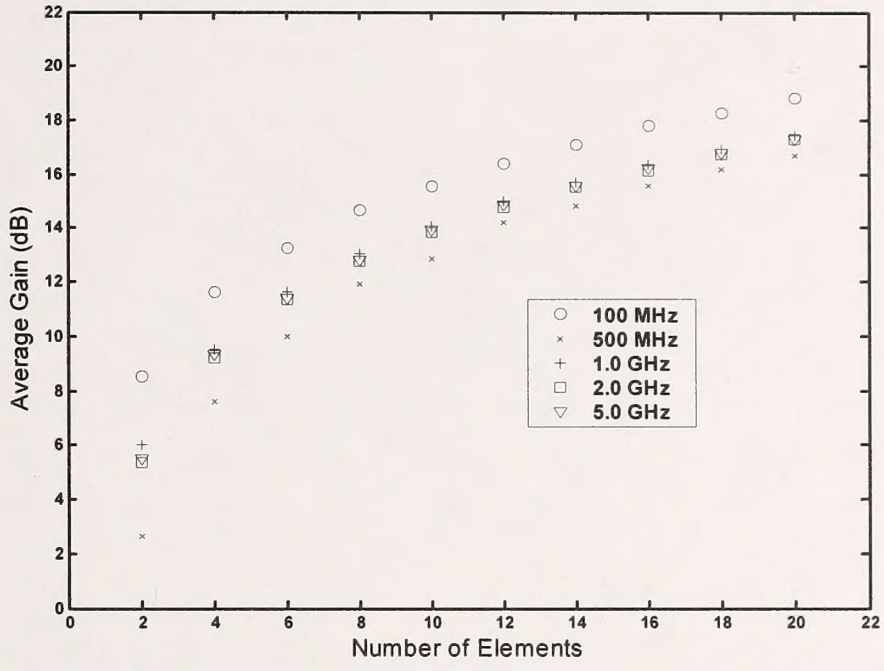

Figure 32. Average gain using 24 trials and 1000 random observation positions over 16 m × 16 m square area in the z = 1.3 m plane.

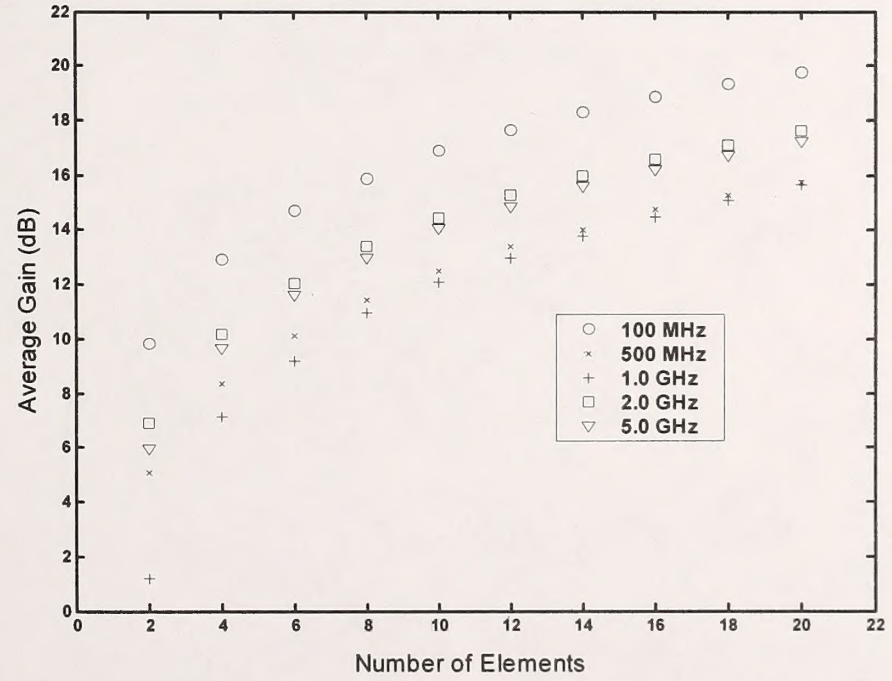

Figure 33. Average gain for 24 trials of 1000 random observation points in the 10 m perimeter of the array.

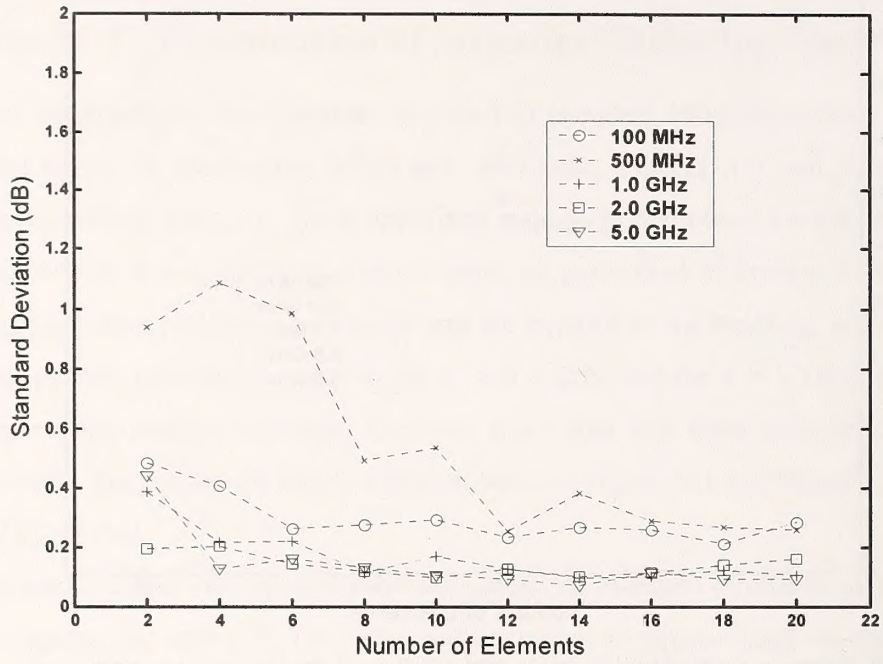

Figure 34. Standard deviation for average gain results in figure 32.

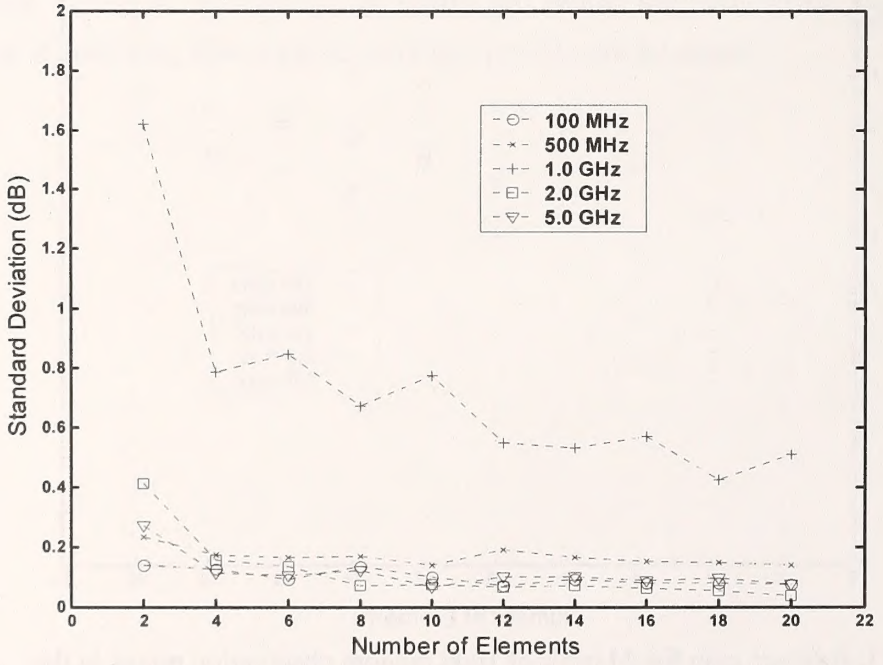

Figure 35. Standard deviation of average gain results shown in figure 33.

NIST Technical Publications

Periodical

Journal of Research of the National Institute of Standards and Technology—Reports NIST research and development in metrology and related fields of physical science, engineering, applied mathematics, statistics, biotechnology, and information technology. Papers cover a broad range of subjects, with major emphasis on measurement methodology and the basic technology underlying standardization. Also included from time to time are survey articles on topics closely related to the Institute's technical and scientific programs. Issued six times a year.

Nonperiodicals

Monographs—Major contributions to the technical literature on various subjects related to the Institute's scientific and technical activities.
Handbooks—Recommended codes of engineering and industrial practice (including safety codes) devel- oped in cooperation with interested industries, professional organizations, and regulatory bodies.
Special Publications—Include proceedings of conferences sponsored by NIST, NIST annual reports, and other special publications appropriate to this grouping such as wall charts, pocket cards, and bibliographies.
National Standard Reference Data Series—Provides quantitative data on the physical and chemical properties of materials, compiled from the world's literature and critically evaluated. Developed under a worldwide program coordinated by NIST under the authority of the National Standard Data Act (Public Law 90-396). NOTE: The Journal of Physical and Chemical Reference Data (JPCRD) is published bimonthly for NIST by the American Institute of Physics (AIP). Subscription orders and renewals are available from AIP, P.O. Box 503284, St. Louis, MO 63150-3284.
Building Science Series—Disseminates technical information developed at the Institute on building materials, components, systems, and whole structures. The series presents research results, test methods, and performance criteria related to the structural and environmental functions and the durability and safety characteristics of building elements and systems.
Technical Notes—Studies or reports which are complete in themselves but restrictive in their treatment of a subject. Analogous to monographs but not so comprehensive in scope or definitive in treatment of the subject area. Often serve as a vehicle for final reports of work performed at NIST under the sponsorship of other government agencies.
Voluntary Product Standards—Developed under procedures published by the Department of Commerce in Part 10, Title 15, of the Code of Federal Regulations. The standards establish nationally recognized requirements for products, and provide all concerned interests with a basis for common understanding of the characteristics of the products. NIST administers this program in support of the efforts of private-sector standardizing organizations.

*Order the **following** NIST publications—FIPS and NISTIRs—from the National Technical Information Service, Springfield, VA 22161.*

Federal Information Processing Standards Publications (FIPS PUB)—Publications in this series collectively constitute the Federal Information Processing Standards Register. The Register serves as the official source of information in the Federal Government regarding standards issued by NIST pursuant to the Federal Property and Administrative Services Act of 1949 as amended, Public Law 89-306 (79 Stat. 1127), and as implemented by Executive Order 11717 (38 FR 12315, dated May 11,1973) and Part 6 of Title 15 CFR (Code of Federal Regulations).
NIST Interagency or Internal Reports (NISTIR)—The series includes interim or final reports on work performed by NIST for outside sponsors (both government and nongovernment). In general, initial distribution is handled by the sponsor; public distribution is handled by sales through the National Technical Information Service, Springfield, VA 22161, in hard copy, electronic media, or microfiche form. NISTIR's may also report results of NIST projects of transitory or limited interest, including those that will be published subsequently in more comprehensive form.

U.S. Department of Commerce
National Bureau of Standards and Technology
325 Broadway
Boulder, CO 80305-3328